Computational Diffusion MRI: Optimal Gradient Encoding Schemes

MOHAMMAD ALIPOOR

CHALMERS

Department of Signals and Systems
CHALMERS UNIVERSITY OF TECHNOLOGY
Göteborg, Sweden 2016

Computational Diffusion MRI: Optimal Gradient Encoding Schemes
MOHAMMAD ALIPOOR

ISBN 978-91-7597-283-1

Doktorsavhandlingar vid Chalmers Tekniska Högskola
Ny serie nr 3964
ISSN 0346-718X

Division of Signal Processing and Biomedical Engineering
Department of Signals and Systems
Chalmers University of Technology
SE-412 96 Göteborg, Sweden
Phone: +46 (0)31 772 5186
E-mail: alipoor@chalmers.se,
mohammad.alipoor@ymail.com

This thesis has been prepared using LaTeX.
Printed by Chalmers Reproservice
Göteborg, Sweden, 2016

To Maryam and Nima

Abstract

Diffusion-weighted magnetic resonance imaging (dMRI) is a non-invasive structural imaging technique that provides information about tissue micro-structures. Quantitative measures derived from dMRI reflect pathological and developmental changes in living tissues such as human brain. Such parameters are increasingly used in diagnostic and prognostic procedures and this has motivated several studies to investigate their estimation accuracy and precision. The precision of an estimated parameter is dependent on the applied gradient encoding scheme (GES). An optimal GES is one that minimizes the variance of the estimated parameter(s). This thesis focuses on optimal GES design for the following dMRI models: second and fourth-order diffusion tensor imaging (DTI), ADC imaging and diffusion kurtosis imaging (DKI). A unified framework is developed that comprises three steps. In the first step, the original problem is formulated as an optimal experiment design problem. The optimal experiment design is the one that minimizes the condition number (K-optimal) or the determinant (D-optimal) of the covariance matrix of the estimated parameters. This yields a non-convex optimization problem. In the second step, the problem is re-formulated as a semi-definite programming (SDP) problem by introducing new decision variables and convex relaxation. In the final step, the SDP problem is solved and the original decision variables are recovered. The proposed framework is comprehensive; it can be applied to DTI, DKI, K-optimal design, D-optimal design, single-shell and multi-shell acquisitions and to optimizing directions and *b*-values.

The main contributions of this thesis include: (i) proof that by uniformly distributing gradient encoding directions one obtains a D-optimal design both for DKI and DTI; (ii) proof that the traditionally used icosahedral GES is D-optimal for DTI; (iii) proof that there exist rotation-invariant GESs that are not uniformly distributed; and (iv) proof that there exist GESs that are D-optimal for DTI and DKI simultaneously. A simple algorithm is presnted that can compute uniformly distributed GESs. In contrast to previous methods, the proposed solution is strictly rotation-invariant. The practical impact/utility of the proposed method is demon-

strated using Monte Carlo simulations. The results show that the precision of parameters estimated using the proposed approach can be as much as 25% better than that estimated by state-of-the-art methods. Validation of these findings using real data and extension to non-linear estimators/diffusion models provide scope for future work.

Keywords: Diffusion MRI, Gradient Encoding Scheme, Diffusion Tensor Imaging, Diffusion Kurtosis Imaging, ADC imaging, D-optimal experiment design, Optimal Image acquisition, Second and Fourth Order Tensors.

Preface

This thesis is in partial fulfillment of the requirements for the degree of Doctor of Philosophy at Chalmers University of Technology, Gothenburg, Sweden.

The work herein was jointly performed in the Signal Processing Group, in the Department of Signals and Systems at Chalmers University of Technology, and MedTech West located at Sahlgrenska University Hospital (both in Gothenburg, Sweden) between August 2011 and December 2015. It was performed under joint supervision of Professor Irene Yu-Hua Gu, Professor Stephan E. Maier, Associate Professor Andrew Mehnert and Associate Professor Göran Starck. Prof. Irene Gu is the main supervisor and examiner of the thesis.

This work was supported in part by Chalmers University of Technology, Sweden and the Iranian Ministry of Science, Research and Technology.

List of Publications

This thesis is based on the following papers:

Paper A: M. Alipoor, I. Y. H. Gu, S. E. Maier, G. Starck, A. Mehnert, 'Optimal Gradient Encoding Schemes for Tensor-based Diffusion Imaging: A Unified Approach', Submitted to Journal.

Paper B: M. Alipoor, I. Y. H. Gu, A. Mehnert, S. E. Maier, G. Starck, 'K-Optimal Gradient Encoding Scheme for Fourth Order Tensor-based Diffusion Profile Imaging', *BioMed Research International*, Volume 2015, Article ID 760230, 10 pages.

Paper C: M. Alipoor, I. Y. H. Gu, S. E. Maier, G. Starck, A. Mehnert, F. Kahl, 'Optimal Gradient Encoding Schemes for Diffusion Tensor and Kurtosis Imaging', Submitted to Journal.

Paper D: M. Alipoor, S. E. Maier, I. Y. H. Gu, A. Mehnert, F. Kahl, 'Optimal Experiment Design for Mono-exponential Model Fitting: Application to Apparent Diffusion Coefficient Imaging', Accepted for *BioMed Research International*, Special issue on *Quantitative Biomedical Imaging: Techniques and Clinical Applications*, 2015.

Paper E: M. Alipoor, I. Y. H. Gu, 'Icosahedral gradient encoding scheme for an arbitrary number of measurements', IEEE 12th International Symposium on Biomedical Imaging:From Nano to Macro, ISBI 2015, New York, pp. 959-962, 2015.

Paper F: M. Alipoor, I. Y. H. Gu, 'Determinant of the information matrix: a new rotation invariant optimality metric to design gradient encoding schemes', IEEE 12th International Symposium on Biomedical Imaging:From Nano to Macro, ISBI 2015, New York, pp. 462-465, 2015.

Paper G: M. Alipoor, I. Y. H. Gu, A. Mehnert, G. Starck, S. E. Maier, 'A novel framework for repeated measurements in diffusion tensor imaging', Submitted to Journal.

Paper H: M. Alipoor, I. Y. H. Gu, A. J. H. Mehnert, Y. Lilja, D. Nilsson, 'Optimal Diffusion Tensor Imaging with Repeated Measurements', In Kensaku Mori, Ichiro Sakuma, Yoshinobu Sato, Christian Barillot, and Nassir Navab, editors, MICCAI (1), volume 8149 of Lecture Notes in Computer Science, pages 687-694. Springer, 2013.

Other publications by the author, not included in the thesis:

U. Ferizi, B. Scherrer, T. Schneider, M. Alipoor, O. Eufracio, R. H.J. Fick, R. Deriche, M. Nilsson, A. K. Loya-Olivas, D. H.J. Poot, A. Ramirez-Manzanares, M. Rivera, A. Rokem, C. Potter, R. F. Dougherty, K. Sakaie, C. Wheeler-Kingshott, T. Witzel, L. L. Wald, S. Warfieldd, J. G. Raya, D. C. Alexander, 'Diffusion MRI Microstructure Models with *in vivo* Human Brain Connectom Data: Results from a Multi-group Comparison', To be submitted to *NeuroImage*.

M. Alipoor, I. Y. H. Gu, A. J. H. Mehnert, Y. Lilja, D. Nilsson, 'On High Order Tensor-based Diffusivity Profile Estimation', In proceedings of 35th Annual International Conference of the IEEE EMBS, pp. 93-96, Osaka, Japan, 3 - 7 July, 2013.

A part of this paper also appears in:
M. Alipoor, I. Y. H. Gu, A. J. H. Mehnert, Y. Lilja, D. Nilsson, 'Weighted Least Squares Estimation of 4th Order Diffusion Tensors', MICCAI 2013 Workshop on Computational Diffusion MRI, Part V, Abstracts from Diffusion MRI modeling Challenge, Nagoya, Japan, 22-26 September, 2013.

M. Alipoor, I. Y. H. Gu, A. J. H. Mehnert, Y. Lilja, D. Nilsson, 'A Novel framework for high order tensor-based diffusivity profile estimation', In Proc. Swedish Symposium on Image Analysis (SSBA 2013), pp. 4-7, Gothenburg, Sweden, 14-15 March, 2013.

Q. Mahmood, M. Alipoor, A. Chodorowski, A. J. H. Mehnert and M. Persson, 'Multi-modal MR Brain Segmentation Using Bayesian-based Adaptive Mean-Shift (BAMS)', MICCAI Grand Challenge on MR Brain Image Segmentation Workshop 2013, Nagoya, Japan, 22-26 September, 2013.

Acknowledgments

I would like to express my sincere gratitude to my supervisors for their patience and support. I always have been lucky to have great teachers. First and foremost, I express my deep gratitude to Prof. Irene Gu who has been patient with me and helped me to get started and to progress. Irene, thank you for being caring, supportive, compassionate and visionary. Next, my heart-felt thanks goes to Andrew Mehnert who has always been more than a co-supervisor. I also would like to express my great appreciation to Prof. Stephan Maier (Department of Radiology, Sahlgrenska University Hospital) and Assoc. Prof. Göran Starck (MRI centre, Sahlgrenska University Hospital) who have joined the supervising team since 2014. I would like to thank Prof. Fredrik Kahl, a co-author of my recent papers, whom I wish I would have known earlier.

On my way, a number of nice people have supported and helped me. In particular, I thank my clinical collaborators/co-authors Dr. Daniel Nilsson and Dr. Ylva Lilja. They have been helpful in balancing my engineering point of view with a medical/clinical understanding. I am very grateful to Dr. Behrooz Nasihatkon who has been open to any technical discussion even those starting with my stupid questions. All these collaborations were made possible through MedTech West which was to facilitate such connections between the health care sector, industry and academia. I would like to thank MedTech West and my lovely colleagues there who have created an inspiring research environment.

Tusen Tack to Tomas McKelvey for his great teaching (I had two courses with him) and group leading skills. I am thankful to all my colleagues at signal processing group and in particular to Ashkan for being open to technical discussions. Without adminstrative staff, our department wouldn't function as it should. So, many thanks to you all. My special thanks goes to Ann-Christine Lindbom who helped me to survive an accident on 20th March 2015. Prof. Mikael Persson, thank you for caring and supporting my PhD studies (and thanks for interviewing me for this PhD studentship).

I would like to thank all my friends (from Chalmers and MedTech West) for

all those nice moments and memories. Thanks to Behrooz, Mehrdad, Alireza, Hamed, Qaiser, Marcus, Ramin, Babak, Hamidreza, Ashkan, Pegah, Bushra, Sofia, Yixiao, Aidin and Maryam, Abbas, Sadegh, Kamran, Faisal, Hakan, Henrik, ... (my apologies if I have forgotten some of you). I extend special thanks to Yazdan who has been more than a friend, supportive and helpful since my first days at Chalmers. I also would like to thank fairly large Iranian community living in Gothenburg who have never let me feel homesick. Last but not the least, I would like to thank my family for their unsparing support and care. All the above mentioned support would have been useless without the love and patience of my beloved wife, Maryam, and my little son, Nima. Thank you all for 4.5 years of exciting and joyful mixture of life and research.

Mohammad Alipoor
Gothenburg, 15 December 2015

Abbreviations and Acronyms

ADC	Apparent Diffusion Coefficient
CSF	Cerebro-spinal Fluid
CN	Condition Number
CRLB	Cramer-Rao Lower Bound
dMRI	Diffusion-weighted MRI
DKI	Diffusion Kurtosis Imaging
DWI	Diffusion-weighted Image/Imaging
DT	Diffusion Tensor
dODF	Diffusion ODF
DTI	Diffusion Tensor Imaging
DSI	Diffusion Spectrum Imaging
DSM	Downhill Simplex Method
DDSD	Distribution of diffusion sensitizing Directions (over unit sphere)
DSE	Diffusion Signal Estimator
DOT	Diffusion Orientation Transform
ED	Equidistant
EDP	Experiment Design Problem

ER	Electrostatic Repulsion
FA	Fractional Anisotropy
fODF	Fiber ODF
GCRLB	CRLB obtained using Gaussian noise assumption
GES	Gradient Encoding Scheme
GT	Global Tractography
GM	Gray Matter
HOT	High Order Tensor
HARDI	High Angular Resolution Diffusion Imaging
LS	Least Squares
LLS	Linear LS
LSE	LS estimator
MD	Mean Diffusivity
MCN	Minimum Condition Number
MRI	Magnetic Resonance Imaging
MLE	Maximum Likelihood Estimator
NNLS	Non-negative Least Squares
NEX	Number of Excitations
NSA	Number of Signal Averages
ODF	Orientation Distribution Function
PAS-MRI	Persistent Angular Structure MRI
PDD	Principal Diffusion Direction
PDF	Probability Density Function
PSD	Positive Semi-Definite
QBI	Q-ball Imaging

RBD	Real Brain Data
SA	Simulated Annealing
SNR	Signal-to-Noise Ratio
TEF	Tensor Estimation Framework
UD	Uniformly Distributed
WLS	Weighted Least Squares
WM	White Matter

Contents

Part I
Introductory Chapters

CHAPTER 1

Introduction

Magnetic resonance imaging (MRI) is a widely used medical imaging technique that acquires images of the body with a technically advanced and expensive scanner. No ionizing radiation is used in MRI and there is no known side effect associated with being scanned by an MRI machine. The technique was developed in 1970s and has been extended to several specialized imaging modalities; e.g. functional MRI and diffusion MRI. The first papers on diffusion MRI date from the mid-1980s [1, 2]. The technique is performed using the same scanner as used in regular MRI (see Figure 1.1). In clinical practice the total scan time should be no more than 10 minutes [3].

Diffusion MRI is sensitive to diffusion (Brownian motion) of water molecules inside living tissues. Its main clinical application is in brain imaging although it finds application to other parts of the body; e.g. breast and prostate. The basic idea behind diffusion MRI is that knowing the paths that water molecules may travel/diffuse in brain, one can estimate the structure of micro-pipes connecting different parts of the brain. Figure 1.2(a) shows a typical result for diffusion imaging of the whole brain. Note that colors are not real (added by the illustration software). Although it may seem too crowded/fuzzy, one can select special regions of interest to study neural pathways connecting two specific parts as shown in Figure 1.2(b).

The two key concepts in this thesis are *diffusion MRI* and *gradient encoding scheme*. The latter is related to the concept of *experiment design*. Thus, we first briefly introduce diffusion MRI and then we describe the concept of experiment design and its relevance to diffusion MRI. Finally we briefly review related studies and summarize contributions of the thesis.

Figure 1.1: Philips MRI machine at Sahlgrenska University Hospital, Gothenburg, Sweden. The image is taken from [4].

1.1 Diffusion-weighted MRI

The movement of water molecules in living tissues (diffusion) is influenced by the local cellular environment. The idea behind diffusion imaging is that from the measured (bulk) diffusion profile in a voxel, one can obtain important properties of the underlying micro-structure (see Figure 1.3). Diffusion-weighted Magnetic Resonance Imaging (dMRI) is a non-invasive structural imaging technique that measures the hindered/restricted diffusion of water molecules in tissues, thus revealing information about tissue micro-structure. It involves acquiring a series of diffusion-weighted images (DWIs), reconstructing the diffusion profile at each voxel and extracting quantitative features describing the underlying micro-structure. This information is used to differentiate micro-structural differences between different tissues (e.g. between malignant and benign tissues) and to locate and track white matter fibre pathways in the brain. The dMRI technique is variously used for medical imaging of the brain, breast [7, 8], pancreas [9], heart [10] and even the whole body [8].

The main use of dMRI in brain imaging is to: (i) discover changes in white matter (WM) due to development, disease or degeneration [11] and (ii) localise white matter tracts, e.g. in pre-surgical planning. The dMRI technique measures the probability density function (PDF), p, of hydrogen nuclei displacements $\mathbf{r}$ over a fixed time t [12]. The function $p(\mathbf{r}, \mathbf{r}_0)$ represents a six-dimensional image [13] where $\mathbf{r}_0$ denotes voxel position in 3D. The 6D data is usually illustrated as iso-

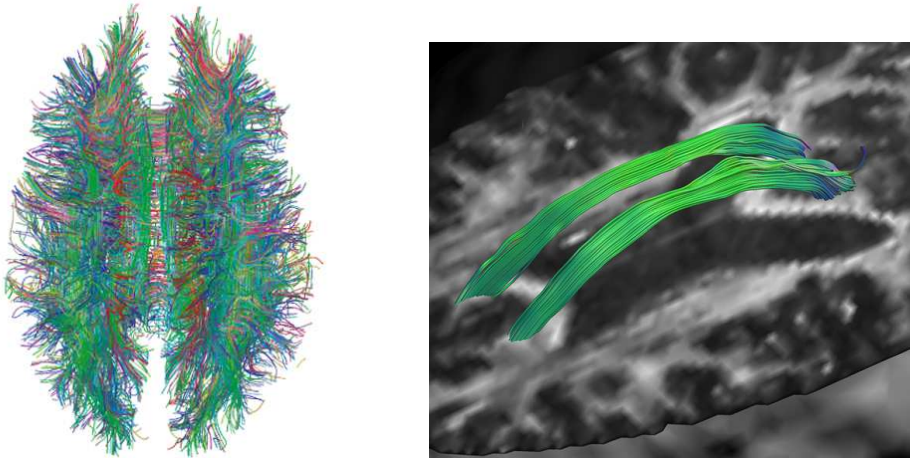

(a) (b)

Figure 1.2: (a) Tracography: mapping fiber pathways (connections) in the human brain. The image is taken from [5]. (b) Tractography visualizations of diffusion MRI in region of interest overlaid on structural MRI: Superior segment of the bilateral cingulum fiber bundles. The image is adapted from [6].

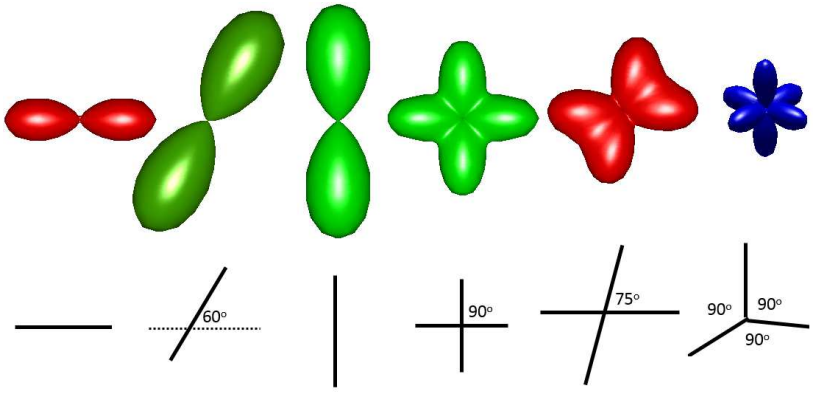

Figure 1.3: Correspondence between underlying micro-structure and the diffusion profile is the basic assumption behind diffusion-weighted MR imaging. First row shows some hypothetical diffusion profiles that arise from the micro-structures presented in the second row.

probability surfaces (see the first row in Figure 1.3). In dMRI it is assumed that p and its features convey useful information about the underlying micro-structure. The diffusion PDF is complex in general, but simple models of diffusion have been proposed to quantify diffusion in living tissues. Among these, the most popular model is the 2nd order diffusion tensor (DT) which was introduced by Basser

et al. [14] to quantify anisotropic diffusion of water molecules in the human brain. Basically, the DT model stems from assuming a zero-mean trivariate Gaussian PDF for the diffusion propagator (p). The (second order positive-definite) DT is defined to be the covariance matrix of p. The well-known limitations of the 2nd order DT in modeling crossing micro-structures has given rise to a variety of complex models including the high-order tensors (HOTs) [15] and diffusion kurtosis imaging [16, 17]. Diffusion tensor imaging (of arbitrary even order, abbreviated by DTI) and diffusion kurtosis imaging (DKI) are of central interest in this thesis. A brief review of the steps involved in brain DWI analysis follows.

The whole task comprises three steps: (i) data acquisition in which one has to choose an acquisition protocol suitable/optimized for the application in consideration; (ii) reconstruction which includes data pre-processing/correction, model fitting, parameter estimation; and (iii) clinical application in which estimated diffusion parameters are used for a clinical study or research advancement. Whilst all three steps are currently being actively researched, the focus of this thesis is on the first step. Before providing more detail about data acquisition in dMRI, we introduce *experiment design* as a general signal processing concept in the following section. This concept is frequently used throughout the thesis.

1.2 Optimal Experiment Design

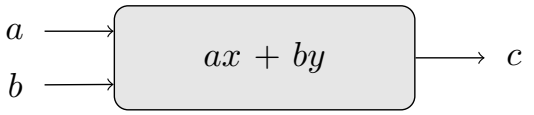

Figure 1.4: A hypothetical experiment design problem with $[a\ b]^T$ as design vector and $[x\ y]^T$ as unknown parameters.

Consider a hypothetical problem in which the task is to estimate x and y, as shown in Figure 1.4. At least two measurements are required to form a linear system as follows:

$$\begin{aligned} a_1x + b_1y &= c_1 \\ a_2x + b_2y &= c_2 \end{aligned} \tag{1.1}$$

The set $\mathfrak{D} = \{[a_1\ b_1]^T, [a_2\ b_2]^T\}$ is called an *experiment design*. For the sake of illustration, let's consider a numerical example with two measurements. Let the true value of the unknown parameters be $[x_0\ y_0]^T = [3\ 2]^T$. Then, two possible experiment designs are $\mathfrak{D}_1 = \{[1\ 1]^T, [5\ 3]^T\}$ and $\mathfrak{D}_2 = \{[-2\ 1]^T, [1\ 2]^T\}$. This numerical example is illustrated in Figure 1.5, where the measurements corresponding to $\mathfrak{D}_1$ and $\mathfrak{D}_2$ are shown by blue and green points/stars, respectively. In

the absence of noise, one can correctly find the unknown parameters using either $\mathfrak{D}_1$ or $\mathfrak{D}_2$. However, in the presence of noise (measurement noise), the problem is not deterministic anymore and designs producing more robust/precise estimates are more favourable. In our example, $\mathfrak{D}_1$ is not a good design as it leads to an ill-conditioned problem. In Figure 1.6 possible measurements using $\mathfrak{D}_1$ (in the presence of Gaussian noise) are plotted. It shows that using $\mathfrak{D}_1$, it is likely to get two parallel lines (means a linear system without solutions) or high variance estimates. Usually, the number of measurements is much higher than the number of unknown parameters ($N > 2$ in this case) to ensure a robust estimation.

To express this in mathematical terms, let us re-write (1.1) as $\mathbf{A}\theta = \mathbf{c}$ where $\theta = [x\, y]^T$, $\mathbf{c} = [c_1\, c_2\, \cdots\, c_N]^T$ and $\mathbf{A}$ is the design matrix (ith row of $\mathbf{A}$ is $[a_i\, b_i]^T$). Thus the least squares (LS) estimate of the unknown parameters $\hat{\theta} = [\hat{x}\, \hat{y}]^T$ is $\hat{\theta} = (\mathbf{A}^T\mathbf{A})^{-1}\mathbf{A}^T\mathbf{c}$. The covariance matrix of $\hat{\theta}$ (assuming Gaussian noise $\mathcal{N}(0, \sigma^2)$) is given by

$$cov(\hat{\theta}) = \sigma^2\mathbf{M}^{-1} \tag{1.2}$$

where $\mathbf{M} = \mathbf{A}^T\mathbf{A}$ is called the *information matrix*. The optimal experiment design entails making the covariance matrix *small* in some sense. It is usual to minimize a scalar function of the covariance matrix. Several scalarization methods have been considered in the literature including D-optimal design (to minimize the determinant of the covariance matrix), E-optimal design (to minimize the spectral norm of the covariance matrix), A-optimal design (to minimize the trace of the covariance matrix) [18] and K-optimal design (to minimize the condition number of the covariance matrix) [19].

Revisiting the numerical example above, one can verify that: (i) the determinant of the information matrix for $\mathfrak{D}_1$ ($\det(\mathbf{M}_1) = 4$) is smaller than that of $\mathfrak{D}_2$ ($\det(\mathbf{M}_2) = 25$); and (ii) the condition number of the information matrix for $\mathfrak{D}_1$ ($\kappa(\mathbf{M}_1) = 322$) is greater than that of $\mathfrak{D}_2$ ($\kappa(\mathbf{M}_2) = 1$). Thus estimates obtained using $\mathfrak{D}_2$ are numerically more stable. In the context of quantitative biomedical imaging, there exist applications where the unknown parameter is a biomarker. In other words, the unknown parameter has diagnostic value and thus the optimal experiment design is essential.

1.3 Experiment Design in dMRI

Irrespective of the diffusion model under consideration, diffusion imaging is an estimation problem whose precision is dependent on the experiment design. Medical applications of diffusion imaging attract wide attention to the problem of optimal experiment design in diffusion-weighted MRI. A short literature review follows.

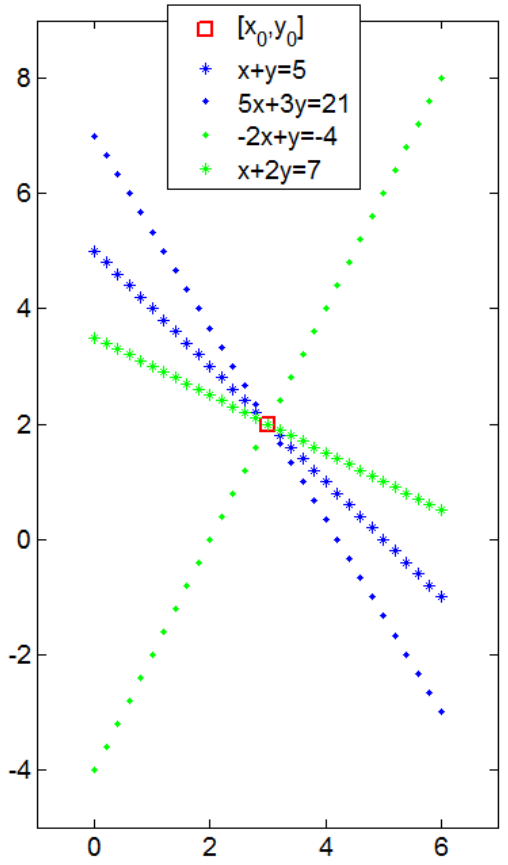

Figure 1.5: A numerical example of the hypothetical estimation problem given in figure 1.4 where the true value of unknown parameters is $[x_0\ y_0]^T = [3\ 2]^T$. Two possible experiment designs are $\mathfrak{D}_1 = \{[1\ 1]^T, [5\ 3]^T\}$ and $\mathfrak{D}_2 = \{[-2\ 1]^T, [1\ 2]^T\}$. In the absence of measurement noise, measurements corresponding to $\mathfrak{D}_1$ and $\mathfrak{D}_2$ are illustrated by the blue and green points/stars, respectively.

At least six measurements in non-collinear directions are required to reconstruct a 2nd order symmetric DT. These measurement directions are called gradient encoding directions. The dMRI signal is measured by applying a diffusion sensitizing gradient in (at least) six different directions. The number and distribution of these directions (over the unit sphere) are elements of the set of acquisition parameters called the gradient encoding scheme (GES). The number of measurements is limited/determined by the clinically feasible time while the distribution of directions in a GES must be optimized for robust estimation of the diffusion parameters. The optimal GES design is one of the most fundamental problems in

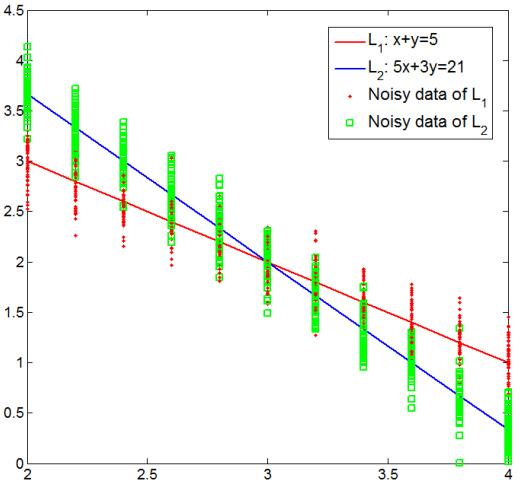

Figure 1.6: A numerical example of the hypothetical estimation problem given in figure 1.4 where bad experiment design $\mathfrak{D}_1 = \{[1\ 1]^T, [5\ 3]^T\}$ can lead to an ill-conditioned system or high variance estimates. The measurement noise is Gaussian distributed as $\mathcal{N}(0, \sigma^2)$ with $\sigma = 0.2$.

dMRI. The classical case, i.e. data acquisition with a constant *b*-value[1] and 2nd order DT reconstruction has been the subject of much study over the last decades [20, 21, 22, 23, 24, 25, 26, 27]. An observation drawn from the literature is that it is widely accepted that measurement directions should be uniformly distributed over the unit sphere. The motivation is that the SNR of measured signal is dependent on the orientation and anisotropy of the tensor [28, 29]. Thus, when the SNR in different directions is unknown, uniformly distributing the diffusion encoding directions ensures an acceptable SNR/performance on average. Although this is intuitively appealing, it has not been mathematically proved.

A review of the literature reveals that:
(i) It is known that the optimal GES is dependent on the diffusion model and the choice of reconstruction method [30]. The common practice of using a uniformly distributed (UD) GES seems to be primarily motivated/tested for the 2nd order DT model [31, 28]. Nevertheless, the UD GES has been extensively used for other models of diffusion imaging (e.g. for DKI [17]);
(ii) There is no exact solution to the problem of uniformly distributing an arbitrary number of points on the unit sphere. The icosahedral scheme [32, 33] gives the solution for certain specific cases. There exist methods that closely approximate the icosahedral scheme and provide solutions for an arbitrary number of measurements. The most important of these is the Jones scheme [28];

[1] so-called single-shell sampling

(iii) The absence of a mathematical proof for the optimality of the UD design has triggered a second round of studies on the optimal design for the 2nd order DT model (a decade after the first round). More recent studies [34, 35] define the optimality based on mathematical metrics borrowed from the experiment design theory;
(iv) A large number of new diffusion models have been proposed to either detect crossing micro-structures [36, 15, 37] or discover more detailed micro-structural information [38, 39, 40]. Despite their promising results, the problem of optimal GES design for the new models as well as multi-shell acquisitions has not, to date, been well-studied [29]. Presumably this is because of the non-convexity and complexity of the problem. Another possible reason is that one obtains satisfactory results using the existing UD GESs; and
(v) Parameters derived from the modern diffusion models are increasingly used as biomarkers in medical diagnosis/prognosis. This has given rise to numerous recent studies exploring optimal GES design for high order models [41, 42, 43] and multi-shell acquisitions [44, 45, 46].

As mentioned above, the optimal GES design in dMRI is a fundamental yet complex problem. Several design approaches have been proposed in the literature. One approach is to consider a simplified diffusion model [34, 42]. Another is to acquire a priori knowledge of the imaged micro-structures using a preliminary scan [43, 34] and exploit this knowledge for GES design [35, 34]. Several researchers have used stochastic optimization techniques for experiment design in dMRI [43, 41, 47, 42]. For instance, in [35] and [43] simulated annealing (SA) is used in experiment design for spinal cord imaging and the downhill simplex method (DSM) is used for K-optimal design in DTI [47]. Although these methods are promising, a drawback they have in common is that a globally optimal solution is not guaranteed. This is because of several simplifications/discretizatios and the use of stochastic optimization techniques.

The optimal GES for each diffusion model is the one that minimizes the variance of the estimated parameters. Using experiment design theory, one can obtain the optimal GES by minimizing the covariance matrix of the estimated parameters in some sense. Possibilities include K-optimal, A-optimal, D-optimal and E-optimal designs. The earliest study that utilized experiment design methods to solve GES design problem is [47], where the K-optimal design problem for 2nd order DTI is solved using DSM. A major drawback of this approach is that it yields a rotationally variant GES[2]. In [35] the A-optimal design problem for 2nd order DTI is solved using SA. In [34], a D-optimal design for 2nd order DTI is presented that assumes a prior knowledge of the micro-structure of interest is available.

[2]For a discussion of the importance of rotation-invariance see Section 2

1.4 Main Contributions

In this thesis, the problem of optimal GES design for dMRI is revisited. A mathematical framework is proposed to solve the optimal GES design problem for even order diffusion tensor imaging and for diffusion kurtosis imaging. Numerous theoretical results are presented that collectively broaden our understanding of different aspects of the GES design problem. In addition to several findings that complement or support previous research, this thesis presents several new results: (i) there exist designs that are optimal for second and fourth order diffusion tensor imaging at the same time; (ii) there exist optimal designs that are optimal for second and fourth order diffusion tensor imaging and DKI at the same time; (iii) the traditionally used icosahedral scheme (as a UD GES) is D-optimal for second and fourth order diffusion tensor imaging and DKI, simultaneously; and (iv) the D-optimal design guarantees rotation invariance of a GES for DTI and DKI.

The proposed method differs from previous studies in the following respects (i) unlike [35, 47], it does not utilize stochastic optimization techniques; (ii) In contrast to [34, 35], it does not assume any simplification/discretization of the original problem; (iii) unlike [35, 34, 47], it provides theoretical and practical properties of the obtained solutions; (iv) In comparison to [28], it produces rotation-invariant schemes (in the case of D-optimal design); and (v) it establishes a general theoretical framework for GES design by extending the proposed method to the modern diffusion imaging techniques such as HOT and DKI.

1.5 Aims and Objectives

This thesis has the following aims: (i) to provide new insights and understanding with respect to the different aspects of optimal gradient encoding schemes in dMRI; and (ii) to develop a unified framework to solve the optimal GES design problems in dMRI. To this end, the thesis has the following objectives:

1. To develop an optimal GES for the second order DTI.

2. To develop an optimal GES for fourth order DTI (does not require multi-shell acquisition).

3. To develop an optimal GES for some high order models that require multi-shell acquisitions.

4. To evaluate the proposed optimal designs in comparison to several state-of-the-art methods.

1.6 Scope of the Thesis

As implied by the aims and objectives, the scope of this thesis is limited to acquisition of dMRI data. It does not include any contribution to other parts of dMRI analysis pipeline. Both single-shell and multi-shell acquisition strategies are considered. The work presented herein is limited to even[3] order diffusion tensor imaging, diffusion kurtosis imaging and apparent diffusion coefficient imaging.

1.7 Thesis Outline

This thesis is organized as follows. The first part, the introductory chapters, includes a brief review of the theory and background of dMRI (Chapter 2), a summary of the thesis work (Chapter 3), and conclusions and future work (Chapter 4). The second part includes appended papers.

[3]This ensures that the HOT is antipodally symmetric.

CHAPTER 2

Background and Theory

This chapter briefly reviews the theoretical underpinnings of dMRI. The chapter begins by reviewing the physiological and physical bases of dMRI. This is followed by a presentation of the mathematical formulation of a simple 2nd order DT model. Next, a review of the related work on two major steps of dMRI processing, namely acquisition and reconstruction, is presented and open questions and shortcomings highlighted. In particular, we review optimal GES design methods and elaborate on the differences and drawbacks of existing approaches. Finally, a brief overview of dMRI applications, such as tractography, is presented.

2.1 Physiology

The human brain has 100 billion neurons (highly specialised neural cells) which together are responsible for regulating most of our activities [48]. A typical neuron is composed of a cell body, dendrites, axon and axon terminals (as shown in Figure 2.1). Axons are surrounded by a fatty tissue, the so-called Myelin sheath, that provides electrical insulation and facilitates signal transmission. The human brain mainly consists of three tissue types, namely white matter (WM), gray matter (GM) and cerebrospinal fluid (CSF). The GM (also known as cortex) is primarily composed of neuron cell bodies while the WM contains myelinated axons that facilitate communication between various regions of the cortex [49]. Myelin is white in color, and the tissue containing the cell bodies is gray in color and this in turn is why their surrounding tissues have their characteristic names. The axons in WM are highly ordered and densely packed into bundles known as fibre tracts or

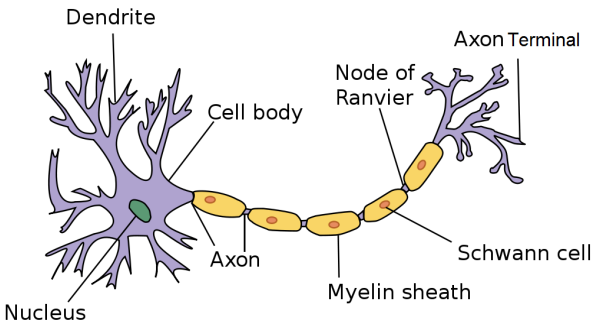

Figure 2.1: A typical neuron consists of the cell body, dendrites, axon (covered by Myelin sheath) and axon terminal. This image is adapted from [50].

fascicles. These white matter fibres connect different cortical (grey matter) areas, and some of them also project down to the spinal cord [49]. The diffusion of water molecules in CSF is isotropic (same in all directions) while in highly structured WM, it is anisotropic reflecting the underlying micro-architecture.

2.2 Physics

It is difficult (if not impossible) to quantify the Brownian motion of a single water molecule. However, considering statistics of the displacements of a huge number of molecules leads to the definition of the diffusion coefficient (for isotropic diffusion). The mean square displacement of the molecules in an isotropic medium is related to their diffusion coefficient according to Einstein's equation: $D = \frac{1}{6t} < \mathbf{r}^T \mathbf{r} >$ where t is diffusion time, $\mathbf{r}$ is the net displacement vector of a particle and $<>$ means the ensemble average [48]. The scalar constant D depends on the properties of the diffusing particles and the medium but not on the direction [48]. In biological tissues the diffusion pattern is modulated by the surrounding microstructure leading to an anisotropic diffusion profile. In the anisotropic case, the probability density function p of displacements x of the particle of interest over a fixed time t describes/quantifies the ongoing diffusion process. Although this PDF is complex in general, some simple models have been proposed to describe anisotropic diffusion; the most important of them is the DT model proposed by [14]. The PDF p and its features reflect the underlying micro-structure. In the literature this is generally taken to be a one-to-one relation meaning that given the micro-structure, the function p can be uniquely characterized and vice versa.

2.3 Mathematics of Diffusion MRI

It has been shown that the diffusion-weighted signal is the Fourier transform of the ensemble average diffusion propagator, $p(\mathbf{r}|t)$ [12, 51, 52, 48]:

$$S(\mathbf{q}) = S_0 \int p(\mathbf{r}|t) exp(i\mathbf{q}.\mathbf{r}) d\mathbf{r} \tag{2.1}$$

where the vector $\mathbf{q}$ is defined as $\mathbf{q} = \gamma\delta\mathbf{Q}$, with $\mathbf{Q}$ being the vector of the applied diffusion gradient, γ is the gyromagnetic ratio of proton (or the hydrogen nucleus) and δ is the diffusion gradient pulse duration (see [12, 52, 48] for more details). The local advection velocity is assumed to be zero (net motion of the whole population) [12] leading to the antipodal symmetry of the diffusion PDF, $p(\mathbf{r}|t) = p(-\mathbf{r}|t)$. The basic DT model for diffusion stems from assuming a zero-mean trivariate Gaussian PDF for the diffusion propagator:

$$p(\mathbf{r}|t) = \frac{1}{\sqrt{(4\pi t)^3|\mathbf{D}|}} exp(-\frac{\mathbf{r}^T\mathbf{D}^{-1}\mathbf{r}}{4t}). \tag{2.2}$$

Under this assumption (2.1) reduces to: $S(\mathbf{q}) = S_0 exp(-t\mathbf{q}^T\mathbf{D}\mathbf{q})$. It is usual to further simplify this notation by introducing variables $\mathbf{g} = \frac{\mathbf{q}}{|\mathbf{q}|}$ and $b = t|\mathbf{q}|^2$ (known as the *b*-value) such that [52, 48]:

$$S(\mathbf{g}) = S_0 exp(-b\mathbf{g}^T\mathbf{D}\mathbf{g}) \tag{2.3}$$

In this perspective, the (second order positive-definite) DT (denoted by $\mathbf{D}$) is the covariance matrix of p. Having six unknowns requires at least six measurements to estimate the DT. As implied by the antipodal symmetry of p, in the absence of noise, the diffusion signal is real-valued. However, this is not the case in practice where the diffusion signal is assumed to be biased by Rician noise. The measured magnitude signal is expressed as [53]:

$$S_n = \sqrt{(S+n_1)^2 + n_2^2} \tag{2.4}$$

where n_1 and n_2 are uncorrelated zero-mean Gaussian noise variables with equal variance. Second order DT estimation leads to an over-determined system of linear equations as follows. Given a set of $N > 6$ DW measurements stored in $\mathbf{y}$, where $y_i = -b^{-1}ln(\frac{S_i}{S_0})$[1], and diffusion sensitizing gradient vectors $\mathbf{g}_i = [g_{ix}, g_{iy}, g_{iz}]$, $i = 1, ..., N$, the DT is given by $\mathbf{d} = \mathbf{G}^{-1}\mathbf{y}$ where $\mathbf{d} = [D_{zz}, D_{yz}, D_{yy}, D_{xz}, D_{xy}, D_{xx}]^T$ and the i^{th} row of $\mathbf{G}$ (known as the design matrix or encoding ma-

[1]The term $-b^{-1}ln(\frac{S}{S_0})$ is referred to as the apparent diffusion coefficient (ADC).

trix) is $[g_{iz}^2, 2g_{iy}g_{iz}, g_{iy}^2, 2g_{ix}g_{iz}, 2g_{ix}g_{iy}, g_{ix}^2]$. In this linear least squares (LLS) estimation framework, (i) positive-definiteness of the solution is not guaranteed, and (ii) sensitivity of the estimated DT to the noise in measurements is upper-bounded by the condition number of the design matrix [32].

In addition to the complicated diffusion models, it is usual to estimate some quantitative features that more simply reflect the properties of the tissue segment under consideration. For 2nd order DTI, two well-defined parameters are widely used: Fractional anisotropy (FA) and the principal direction of diffusion (PDD). The FA value is calculated as the normalized variance of eigenvalues (λ_i) of the diffusion tensor:

$$\mathrm{FA} = \sqrt{\frac{3\sum_{i=1}^{3}(\lambda_i(\mathbf{D}) - \bar{\lambda}(\mathbf{D}))^2}{2\sum_{i=1}^{3}(\lambda_i(\mathbf{D}))^2}} \tag{2.5}$$

FA takes a value in the range $[0,1]$, where FA=0 means isotropic diffusion (spherical tensor) and FA=1 indicates extremely anisotropic diffusion (very elongated ellipsoidal tensor). In the white matter of the human brain, as a consequence of the highly structured environment, the FA value is close to one. The FA value is known to reflect the changes related to aging or pathological alterations. The eigen-vector corresponding to the largest eigen-value determines the principal direction of diffusion (PDD) that is used for fiber tracking (tractography).

2.4 Acquisition: GES Design

The analysis of the diffusion signal is closely related to the sampling of *q*-space [54]. Different sampling schemes studied to-date fall into two groups based on their sampling strategy: Cartesian and spherical sampling [11]. Cartesian sampling (also known as full space sampling) is used in diffusion spectrum imaging (DSI) [55]. Full sampling of *q*-space requires a high number of measurements ($N > 200$) and thus is not practicable *in vivo* because of the long acquisition time. Spherical sampling strategies (also known as high angular resolution imaging (HARDI) techniques) are divided into two groups: single-shell and multiple-shell. Single-shell schemes provide samples over a sphere in *q*-space. In other words, a single non-zero *b*-value is applied. In contrast, multiple-shell schemes apply several non-zero *b*-values. [54] categorizes different sampling schemes based on the number of required measurements and adds radial and sparse sampling strategies. In addition to the sampling strategy, the selection of the sampling points is also highly important. For both single and multi-shell sampling, one needs to make a decision about the number of measurements to perform and the distribution of sampling points (the GES).

The minimum number of required measurements is determined, on the one

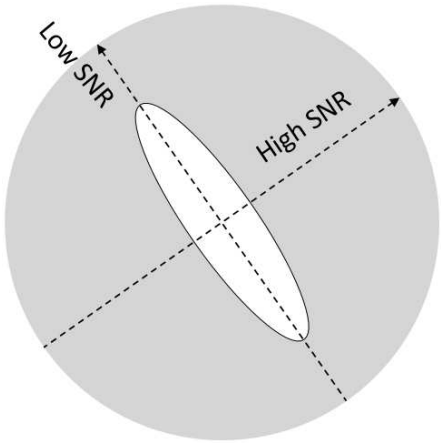

Figure 2.2: Spatially varying SNR in dMRI measurements: High SNR is achieved when measuring perpendicular to the fiber/tensor.

hand, by the number of unknown parameters in our model. On the other hand, the maximum number of measurements is limited by the clinically acceptable acquisition time. Thus, it is the distribution of measurement directions that should be optimized to minimize the variance of the estimated parameters (an experiment design problem).

2.4.1 Model-free GES Design

It is known that all theoretical methods for optimal experiment design (e.g. D-optimal) require the consideration of a diffusion model. However, there exist model-free GESs that are deemed to be optimal for all kinds of diffusion imaging. It is well-accepted that uniformly distributed (UD) gradient encoding schemes are optimal for 2nd order DTI. Further, the UD GES is frequently used for other diffusion models [17, 27, 30, 44] implying that it is the best available choice for any kind of diffusion imaging.

The UD GES is motivated by the fact that SNR of dMRI measurements is spatially varying. The SNR of the measured signal is dependent on the orientation and anisotropy of the imaged tensor [28, 29]. As shown in Figure 2.2, when measuring along the fiber, the signal level drops to the noise floor (according to (2.3)). However, when measuring perpendicular to the fiber, the SNR is much higher [29]. To better visualize the spatially varying SNR, the dMRI signal arising from six hypothetical micro-structures (according to (2.11)) are shown in Figure 2.3. Broadly speaking, measurements in the red areas have a high SNR while measurements in the dark blue area are almost useless (too noisy). Thus, without prior knowledge of the orientation of the structure to be imaged, a uniform distribution of gradi-

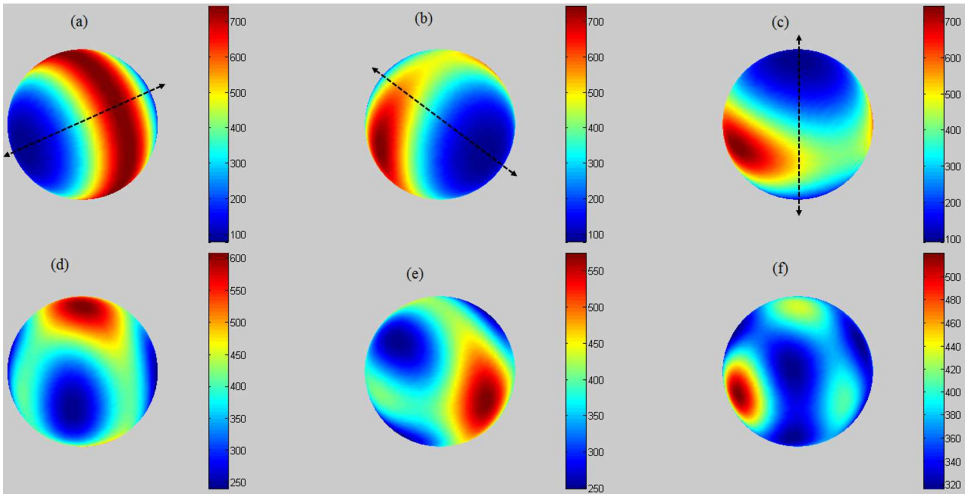

Figure 2.3: Spatially varying SNR in dMRI measurements: dMRI signal arising from six hypothetical micro-structures (a) $\mathbf{D}_1 = \text{diag}([17\ 2\ 2]) \times 10^{-4}$, FA=0.87; (b) $\mathbf{D}_2 = \text{diag}([2\ \ 17\ \ 5]) \times 10^{-4}$, FA=0.77; (c) $\mathbf{D}_3 = \text{diag}([2\ 6\ 16]) \times 10^{-4}$, FA=0.73; (d) $\mathbf{D}_1 + \mathbf{D}_2$; (e) $\mathbf{D}_1 + \mathbf{D}_3$ and (f) $\mathbf{D}_1 + \mathbf{D}_2 + \mathbf{D}_3$. The diffusion signal is simulated using (2.11). The orientation of diffusion tensors are shown with dashed arrows.

ent encoding directions seems sensible. This increases the chance of having at least six high SNR measurements for any micro-structure. Another motivation is that a uniform distribution of gradient encoding directions minimizes the cross-term effects in estimating the diffusion tensor [56]. Although both arguments are intuitively appealing, they have not been mathematically proved.

This thesis, for the first time, proves that a UD GES can be optimal for several different models (i.e. the UD GES conforms to the conditions obtained by model-dependent GES design approaches). For this reason, herein we categorize the GES design methods based on the number of shells (and not the model under consideration). In the following subsection we briefly review some existing work on single-shell optimal GES design that has mainly been devised for second order DTI.

2.4.2 Single-shell GES Design

To estimate parameters of some diffusion models (e.g. even-order tensors) a single-shell data acquisition suffices where only one non-zero *b*-value is used for data acquisition. Although multi-shell acquisitions (with several non-zero *b*-values) can provide additional information [57], single-shell acquisitions are usual because of the acquisition time limit and computational burden.

Given the possibility of making N measurements, one of the most fundamental questions in dMRI is how to distribute sampling points over the unit sphere (for a single-shell acquisition scheme). The optimal single-shell sampling has been widely studied [28, 20, 22, 23, 24, 31, 32, 25, 26, 30, 27]. Four observations can be drawn from the literature:

(i) It is widely accepted among researchers that sampling points should be uniformly distributed over the unit sphere (the motivation is that the SNR of the measured signal is dependent on the orientation and anisotropy of the tensor [28, 29]). There is no analytical solution for the problem of uniformly distributing an arbitrary number of points on a sphere [58]. The icosahedral scheme [24, 32] provides the UD GES for some specific cases. There exist methods to obtain an approximately UD GES for an arbitrary number of points. Of particular note is the electrostatic repulsion (ER) scheme that minimizes the interaction energy of identical charges positioned at sampling points [28]. These two methods (icosahedral and ER) were originally devised for 2nd order DTI but have been used for GES design in DKI and other models of diffusion imaging [27, 30, 44] because they generate an (approximately) uniform distribution of points on a sphere.

(ii) The uniformity of the distribution of gradient encoding directions over the sphere is measured by the minimum angle subtended by any possible pair of encoding directions [44, 56, 24, 58] (denoted by $\beta_{\min}$, defined below). Let β_{ij} be the angle between $\mathbf{g}_i$ and $\mathbf{g}_j$. Then, the minimum and maximum angles, $\beta_{\min}$ and $\beta_{\max}$ are defined as follows:

$$\begin{aligned} \beta_i &= \min\{\beta_{ij} \mid i \neq j,\ j = 1, \cdots, N\}, \\ \beta_{\min} &= \min\{\beta_i \mid i = 1, \cdots, N\}, \\ \beta_{\max} &= \max\{\beta_i \mid i = 1, \cdots, N\}. \end{aligned} \tag{2.6}$$

For each GES, the minimum angular distance between two neighboring points, $\beta_{\min}$ is considered as a measure of uniformity of the distribution of points (the larger, the better). For icosahedral schemes (or exact UD GESs), $\beta_{\min}$ reaches the best possible value $\beta^*_{\min} = \frac{180}{\pi}\arctan(2)\sqrt{\frac{5}{N-1}}$ [58]. This can be used to examine how close a given GES is to the exact UD GES. For ideal GESs (e.g., the icosahedral scheme), $\beta_{\min} = \beta_{\max}$ holds, a smaller value of $\Delta\beta = \beta_{\max} - \beta_{\min}$ implies that the given GES is better in terms of uniformity. It is noteworthy that some other optimality metrics have been proposed to measure the uniformity of the distribution of directions of a GES. These all stem from the idea that minimizing the electrostatic interaction (Coulombic) energy between equal charges positioned on the sphere will uniformly distribute those point charges. Following this idea, several energy functions are defined including J_1 [59, 33, 24], J_2 [44], J_3 [41] and

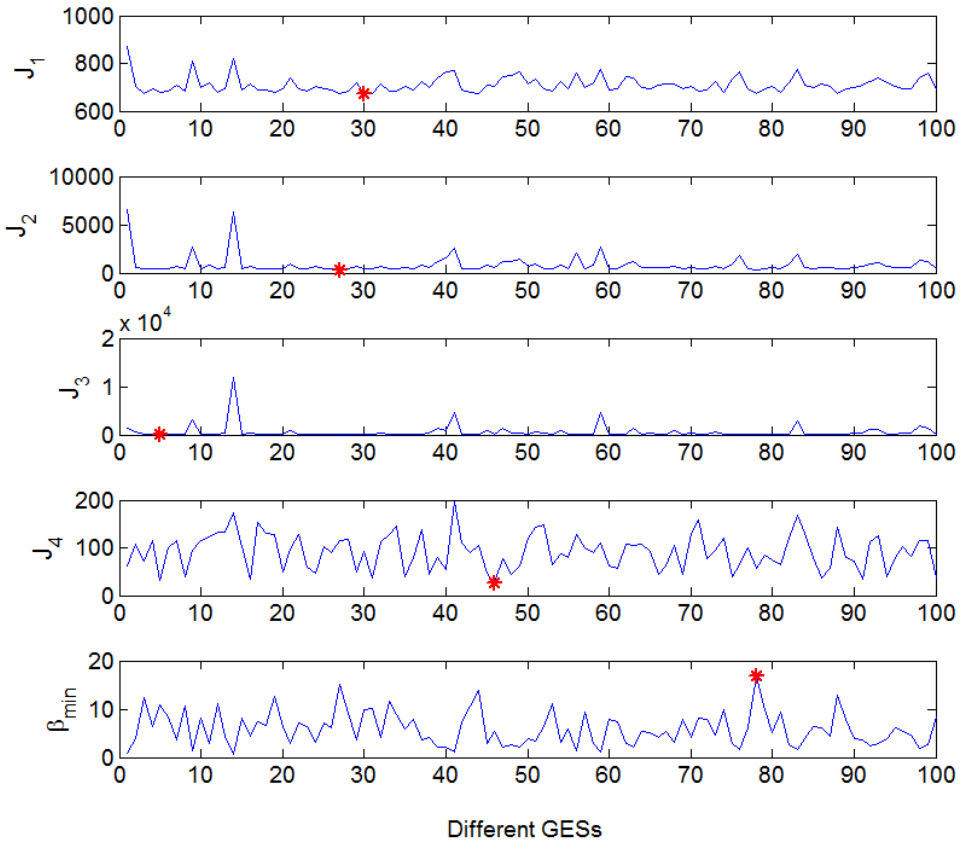

Figure 2.4: Five uniformity metrics are evaluated for 100 GESs (with N=20) obtained by D-optimal design algorithm for 2nd order DTI (given in *Paper A*). See definition of the metrics in the text (for J_4 we set $a = 2$). The optimal GES for each metric is denoted by a red star. It can be seen that optimality in one sense does not require/result in optimality in any other sense. The optimal GESs are #30 ($\beta_{\text{min}} = 9.8^\circ$), #27 ($\beta_{\text{min}} = 15.1^\circ$), #5 ($\beta_{\text{min}} = 10.9^\circ$), #46 ($\beta_{\text{min}} = 5.3^\circ$) and #78 ($\beta_{\text{min}} = 16.8^\circ$).

J_4:

$$\begin{aligned} J_1 &= \textstyle\sum_{i=1}^{2N} \sum_{j=i+1}^{2N} \frac{1}{||\mathbf{g}_i - \mathbf{g}_j||}. \\ J_2 &= \textstyle\sum_{i=1}^{N} \frac{1}{||\mathbf{g}_i - \mathbf{g}_j||^2} + \frac{1}{||\mathbf{g}_i + \mathbf{g}_j||^2}. \\ J_3 &= \textstyle\sum_{i=1}^{2N} \frac{\mathbf{g}_i - \mathbf{g}_j}{||\mathbf{g}_i - \mathbf{g}_j||^3}. \\ J_4 &= \textstyle\sum_{i=1}^{2N} \frac{\mathbf{g}_i - \mathbf{g}_j}{||\mathbf{g}_i - \mathbf{g}_j||^a}. \end{aligned} \tag{2.7}$$

In these cost functions the ith gradient encoding direction of a GES with N points

is denoted by $\mathbf{g}_i$ where the index i varies up to $2N$ when for each $\mathbf{g}_i$ the corresponding $-\mathbf{g}_i$ is also considered (to account for antipodal symmetry). As can be seen J_3 is a vector-valued function. In a private communication, the authors of [41] stated that they minimize $||J_3||$. In J_4 the constant a can be any positive real number. An interesting observation is that these metrics are not consistent, e.g. for two given GESs, $J_1(\text{GES}_1) < J_1(\text{GES}_2)$ does not necessarily lead to $\beta_{\min}(\text{GES}_1) > \beta_{\min}(\text{GES}_2)$. As shown in Figure 2.4 this inconsistency applies to all five above-mentioned metrics. For 100 GESs (N=20) obtained by the D-optimal design method for 2nd order DTI (given in *Paper A*), all five metrics are evaluated and their respective optimal GES is denoted by red stars. It can be seen that optimality in one sense does not require/result in optimality in any other sense. In this thesis, we mainly use $\beta_{\min}$ because it seems a direct and appealing metric.

(iii) It is widely accepted that sampling more points leads to more precise tensor estimation (the motivation for acquiring more measurements is to mitigate noise). For the second order DT model (with only six unknowns) at least 30 measurements are required for robust estimation of all parameters of interest [31].

(iv) Choosing different objective functions leads to different optimal schemes. Minimization of the interaction energy of identical charges positioned at sampling points (known as the ER scheme) [28], minimization of the condition number (MCN) of the design matrix [47] associated with the least squares estimation of the DT, and the icosahedral scheme [32] are popular examples. Several other criteria have also been proposed to measure the optimality of sampling schemes including the total tensor variance [24], signal deviation [27], variance of tensor-derived scalars [32, 31], minimum angle between pairs of encoding directions, and SNR of tensor-derived scalars [60]. The reader is referred to [29] for a comprehensive review of these sampling schemes.

(v) Because of the anisotropic noise propagation in dMRI [32] the rotational variance of any particular performance measure should be evaluated. For a discussion of the importance of rotation-invariance (of a GES) see Chapter 15 in [29]. The importance of rotation-invariance gave rise to a common evaluation framework [31, 22, 32, 27, 47] for sampling schemes (based on the Monte Carlo simulations). This generalized GES evaluation framework (mainly used for the 2nd order DT) is described in Algorithm 1 below. In addition to the FA value, the uncertainty of the vector-valued quantities (e.g. PDD) should be evaluated. We compute the 95% cone of uncertainty (CU_{95} as defined in [61]) to quantify the uncertainty in the estimation of the PDD.

This well-known evaluation framework is applicable when the optimality measure of interest is a function of the DT-derived quantities. In the MCN and Jones schemes the optimality/fitness of a given set of sampling points can be directly evaluated. Thus the framework reduces to successive rotations and evaluations

Algorithm 1: Pseudo-algorithm to compute response surface of σ(FA)

Data: diagonal tensor $\mathbf{D}_0$ with a prescribed FA, N_R rotation matrices, number of Monte Carlo trials N_{MC}, SNR=S_0/σ, GES

Result: response surface of σ(FA)

for $r = 1$ **to** N_R **do**

  Obtain $\mathbf{D} = \mathbf{R}^T\mathbf{D}_0\mathbf{R}$;

  for $n = 1$ **to** N_{MC} **do**

    - simulate the diffusion signal at the sampling points defined by the GES under evaluation using the Stejskal-Tanner [62] equation ($S(\mathbf{g}_i) = S_0 exp(-b\mathbf{g}_i^T\mathbf{D}\mathbf{g}_i)$);

    - add Rician distributed noise to the synthetic signal to obtain given SNR;

    - compute the diffusion tensor $\hat{\mathbf{D}}$ and corresponding FA value;

  record the standard deviation of estimated FA (σ(FA));

to assess the rotational variance. Simulations in [32] show that the icosahedral sampling scheme (detailed in [32]) is superior to the MCN scheme in terms of rotational-invariance of the condition number (CN).

As emphasized in [30], the determination of an optimal GES is dependent on the choice of diffusion model. It is still an open question for many diffusion models. In this thesis, we propose a unified approach for optimal GES design in DTI and show that it can be extended to high order DTI and DKI.

2.4.3 Multi-shell GES Design

Some modern diffusion models (e.g. DKI) require multi-shell acquisitions. Optimal GES design for multi-shell acquisition of dMRI data has also been the subject of numerous studies. Several multi-shell GES design methods are based on single-shell solutions [45, 46, 41]. Other studies have developed model-dependent optimal multi-shell schemes [43, 41, 30]. Direct extension of the ER scheme (introduced in [28]) to obtain an UD multi-shell GES is also investigated [44, 63, 64]. Another extension to the ER algorithm is presented in [65] using tensor metrics and charged containers.

In this thesis, an optimal multi-shell GES is designed for DKI. Furthermore, it is shown that the developed GES is D-optimal for 2nd and fourth order DTI, as well.

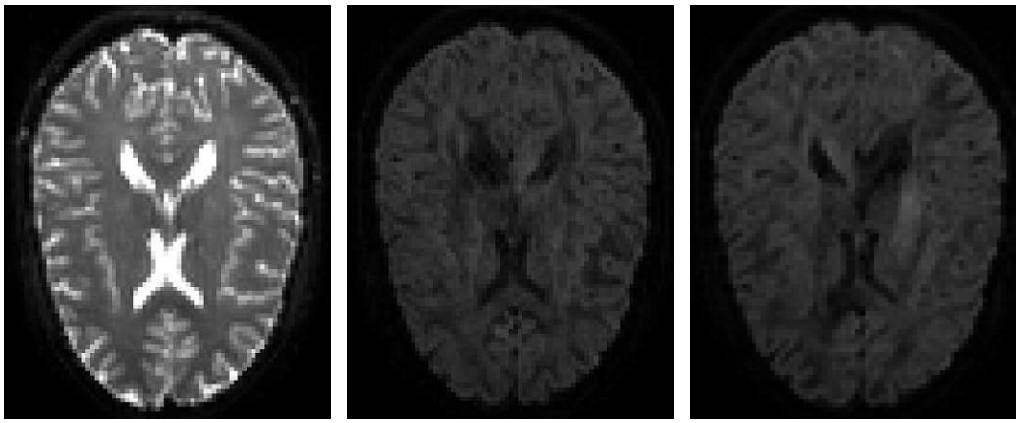

(a) (b) (c)

Figure 2.5: An example of input data for a dMRI reconstruction algorithm: (a) b_0 image of an arbitrary slice of a human brain, (b) same slice when imaged with b=1000 s/mm^2 and $\mathbf{g} = [0.52\ -0.52\ 0.68]$, (c) same slice when imaged with b=1000 s/mm^2 and $\mathbf{g} = [-0.69\ -0.73\ -0.02]$.

2.4.4 GES Design Theory

Given that much of this thesis is concerned with the optimal experiment design for several diffusion imaging techniques, in this section we briefly review experiment design theory. In many different areas of engineering, the problem of estimating a vector $\theta \in \mathbb{R}^n$ from a set of measurements $s_i, i = 1,\ldots,N$ arises, where

$$s_i = \mathbf{a}_i^T \theta + \varepsilon_i, \qquad i = 1,\ldots,N \tag{2.8}$$

$\mathbf{a}_i$ is the design for measurement i and the ε_is are assumed to be independent zero mean random variables with equal variance σ^2 (the measurement noise). The precision of the estimation problem is dependent on the experiment designs $\mathbf{a}_i$, $i = 1,\cdots,N$. The least squares estimator (LSE) is unbiased and has the following covariance matrix [19]:

$$\mathrm{Cov}(\hat{\theta}) = \sigma^2 \mathbf{M}^{-1} \tag{2.9}$$

where $\mathbf{M} = \sum_{i=1}^{N} \mathbf{a}_i \mathbf{a}_i^T$ and is usually called the *"information matrix"*. Optimal experiment design entails making the covariance matrix *small* in some sense. It is usual to minimize a scalar function of the covariance matrix. Several scalarization methods have been studied to date including D-optimal design (to minimize the determinant of the covariance matrix) [43, 34, 42], E-optimal design (to minimize the spectral norm of the covariance matrix) [18], A-optimal design (to minimize the trace of the covariance matrix) [35, 18] and K-optimal design (to minimize the condition number of the covariance matrix) [47, 19].

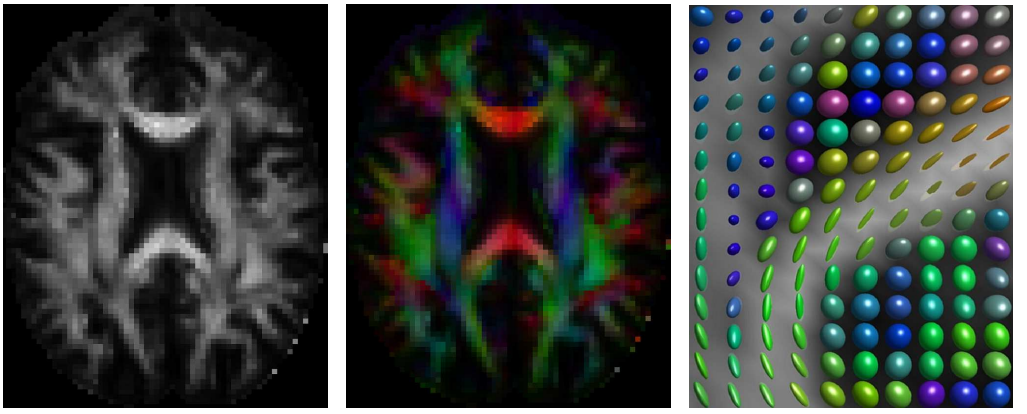

(a) (b) (c)

Figure 2.6: Three examples of outputs of a dMRI reconstruction algorithm: (a) FA map of an arbitrary slice of a human brain, (b) color coded PDD map of the same slice, (c) a hypothetical tensor field. Images (a) and (b) are produced by ExploreDTI [66]. The image (c) is adapted from [67].

2.5 Reconstruction

Given a set of dMRI measurements for each voxel, a reconstruction method is expected to provide:
(i) an estimate of the number of fiber bundles constructing the underlying micro-structure (although it is an input in some methods);
(ii) an estimate of the orientation of each fascicle; and
(iii) features of p that characterize the tissue/micro-architecture properties such as FA.

Example inputs and outputs of a dMRI reconstruction algorithm are illustrated in Figures 2.5 and 2.6, respectively. More sophisticated models would provide orientation distribution functions (ODFs) instead of a tensor field in 2.6(c).

A wide variety of methods have been proposed to analyze the diffusion signal in order to determine the underlying micro-structure and its features. These approaches broadly fall into two groups: parametric (model-based) and non-parametric (model-free) approaches. Parametric methods assume that the dMRI signal is a weighted linear sum of functions each of which models the diffusion pattern of a single fascicle [68]. This group is also known as the mixture models [54, 68]. The non-parametric methods try to estimate some function indicating potential fiber directions and their uncertainty [69]. The target functions are some mathematical series [54] or spherical orientation distribution functions (ODF) [69]. This catego-

rization is widely accepted although there is no clear demarcation between these two groups. For example the Persistent Angular Structure (PAS-MRI) method is classified as a parametric/model-based method in [54] while being considered as non-parametric/model-free in [69, 68]. It is noteworthy that some methods model the ADC profile instead of modeling the diffusion signal. Regardless of the applied method/model, the peaks of the ADC profile do not coincide with fascicle orientations (except for single-fascicle micro-structure) but the profile is useful for FA computation [12]. In this regard, the reconstruction methods are divided into two groups: those that aim to determine the fODF (or its blurred version known as dODF [70]) and those that aim to estimate the ADC profile.

2.5.1 Parametric Methods

The regular DT model is the most popular parametric method that adequately models the diffusion signal within isotropic or single-fascicle voxels. Simple, fast and robust estimation and well-established interpretation framework make the 2nd order DT model suitable for daily clinical use. However, its known limitations in modeling complex micro-structures has given rise to many new models and reconstruction frameworks. A multi-tensor model is a natural generalization of the DT model to resolve complex architectures. Basically it assumes that p is sum of several Gaussian distributions:

$$p(\mathbf{r}|t) = \sum_{i=1}^{n} f_i \, \frac{1}{\sqrt{(4\pi t)^3 |\mathbf{D}_i|}} exp(-\frac{r^T \mathbf{D}_i^{-1} r}{4t}) \tag{2.10}$$

where f_i are volume fractions such that $f_i \in [0,1]$ and $\sum_{i=1}^{n} f_i = 1$. This assumption leads to the multi-exponential modeling of the diffusion signal:

$$S(\mathbf{g}) = S_0 \sum_{i=1}^{n} f_i \, exp(-b\mathbf{g}^T \mathbf{D}_i \mathbf{g}) \tag{2.11}$$

This idea (with some modifications) has led to various multi-compartment models, where each term models the contribution of different biologic compartments (such as intra-axonal, extra-axonal, isotropic and so on) in the diffusion signal (see [71] for details). The main limitations with this family of parametric models are:
(i) Model order selection - to choose a suitable n is not a trivial task in general. Some studies use a fixed n that would lead to poor results in case of a mismatch between the underlying micro-structure and the model (see Figure 27.2 in [29]). Several studies have sought to estimate n separately [12].
(ii) Acquisition requirements - the number of unknown parameters and thereof the

minimum number of measurements depends on n. Further, given a single-shell acquisition, it is impossible to precisely estimate multi-tensor models [11].
(iii) Estimation framework - because of the non-linearities and noisy measurements, the estimation process is challenging.

The model-based approaches usually reveal a finite number of fascicles in each voxel and their respective features (such as FA, principal diffusion direction (PDD)). However, for adequately resolving fanning or branching fascicles, estimation of fODF/dODF would seem to be more desirable. The non-parametric methods seek to estimate a spherical function $fODF : \Omega \rightarrow \mathbb{R}$ for each voxel describing the fraction of fibers pointing in each direction [29] (or conceptually the probability that a particle located in the center of the voxel, will diffuse in that direction). In this perspective, PAS-MRI and deconvolution-based methods are classified as non-parametric methods as they estimate the fODF/dODF, although they use some models of diffusion as the response functions. For a discussion of the advantages and disadvantages of the multi-tensor model see [11] and [54], respectively.

2.5.2 Non-Parametric Methods

Non-parametric DWI reconstruction methods include diffusion spectrum imaging (DSI) [55], q-ball imaging (QBI) [36] and its variations, the diffusion orientation transform (DOT) [72], PAS-MRI [37], deconvolution-based methods [73] and higher order tensor methods [74]. [11] enumerates three major error sources in q-space approaches (DSI,QBI, etc), the most important of which is the acquisition requirements. For more details on the advantages and drawbacks of different methods see [54, 29]. The general drawbacks with model-free approaches are as follows:
(i) The incorporation of the probability in describing diffusion patterns may not be desirable all the time. For some applications, such as tractography or evaluation of synthetic data-based studies, quantification of the number of fascicles and their PDD are required. This has led to an active research area dealing with the extraction of the required deterministic information (e.g. PDD) from the available probabilistic description of the diffusion profile. The research on this secondary problem has led to fODF maxima extraction methods [75, 76, 77], tensor decomposition [78] and Z-eigen decomposition theory [79].
(ii) The model-free approaches describe the general shape of the diffusion pattern rather than describing the contribution of each fascicle and its orientation and anisotropy. Most existing tractography algorithms are based on the model-free reconstructions but still rely on FA maps (obtained from 2nd order DT) to detect white matter tissue.
(iii) The evaluation of these methods (especially on synthetic data) is dependent

on how one interprets them. For example, Z-eigen decomposition of a fourth order tensor gives $v \leq 13$ Z-eigenvalues [80] while in evaluation of angular error, the number of PDDs n is assumed to be known (as in [81]) and only the n largest eigenvalue-vector pairs are considered.

2.5.3 High Order Diffusion Tensors (HOTs)

Non-Gaussian diffusion models have gained wide attention because of their ability/potential to resolve complex fiber architectures such as fiber crossing, branching or kissing. One of the promising alternatives to 2nd order DTI that can model complex fiber architectures in the brain, is the HOT model[2]. In regions with complex micro-structures, HOTs can model the apparent diffusion coefficient (ADC) with higher accuracy than the conventional 2nd order model [84].

Given that optimal GES design for HOTs is one of the contributions of this thesis, this section briefly reviews HOT-based ADC profile estimation. The Stejskal-Tanner equation for dMRI signal attenuation is [62]:

$$-\frac{1}{b}\ln\left(\frac{S}{S_0}\right) = d(\mathbf{g}) \tag{2.12}$$

where $d(\mathbf{g})$ is the diffusivity function, S is the measured signal when the diffusion sensitizing gradient is applied in the direction $\mathbf{g}$, S_0 is the observed signal in the absence of such a gradient, and b is the diffusion weighting factor. (2.12) shows that for the second order DT model $d(\mathbf{g}) = \mathbf{g}^T\mathbf{D}\mathbf{g} \geq 0$. Generally, $d(\mathbf{g}) : \Omega \rightarrow \mathbb{R}^+$. The diffusivity function $d(\mathbf{g})$ (also known as the ADC profile) is modeled using even-order symmetric tensors as follows:

$$d(\mathbf{g}) = \sum_{i_1=1}^{3}\sum_{i_2=1}^{3}\ldots\sum_{i_m=1}^{3} d_{i_1 i_2 \ldots i_m} g_{i_1} g_{i_2} \ldots g_{i_m} \tag{2.13}$$

where the upper bound of the summations shows the tensor dimension and the number of sums is equal to the order of tensor m. Tensor elements are shown with $d_{i_1 i_2 \ldots i_m}$, and symmetry means that any possible permutations of indices gives the same value. For example, for a fourth order symmetric tensor: $d_{1112} = d_{2111} = d_{1121} = d_{1211} = d_{\alpha(3,1,0)}$ where $\alpha(n_1, n_2, n_3)$ shows any possible permutation of indices having n_1 ones, n_2 twos and n_3 threes. Thus each m-th order tensor has $n = (m+1)(m+2)/2$ distinct elements with the multiplicity of $\mu_{\alpha(n_1,n_2,n_3)} = \frac{m!}{n_1!n_2!n_3!}$. In this thesis and related publications, $\mathbf{g} = [x, y, z]$ is used instead of $\mathbf{g} = [g_1, g_2, g_3]$

[2] Variations of HOTs ranked first in both the HARDI reconstruction contest held in conjunction with ISBI 2012 [82] and the diffusion MRI modeling challenge held in conjunction with MICCAI 2013 [83].

for simplicity. Thus, the diffusivity function takes the following form:

$$d(\mathbf{g}) = \sum_{i=0}^{m}\sum_{j=0}^{m-i} t_{h(i,j)} g_1^i g_2^j g_3^{m-i-j} = \sum_{i=0}^{m}\sum_{j=0}^{m-i} t_{h(i,j)} x^i y^j z^{m-i-j} \tag{2.14}$$

where $\mathbf{g} = [g_1\ g_2\ g_3]^T$, $t_{h(i,j)} = d_{\alpha(i,j,m-i-j)}\mu_{\alpha(i,j,m-i-j)}$ and $h(i,j) = j+1+i(2m+3-i)/2$. Thus the diffusivity function can be expressed as an inner product of two vectors, $\mathbf{t}$ containing the unknown diffusion tensor elements and $\mathbf{a}_i$ containing the experiment design for ith measurement:

$$d(\mathbf{g}_i) = \mathbf{a}_i^T \mathbf{t} \tag{2.15}$$

where $\mathbf{g}_i = [x_i, y_i, z_i]$. Both $\mathbf{t}$ and $\mathbf{a}_i$ belong to $\mathbb{R}^n$ but multiplicity coefficients may be placed in either of the vectors. We keep them in experiment design always.

Examples: For $m = 2$, the second order DT model, the diffusivity function is composed of: $\mathbf{t} = [d_{xx}\ d_{yy}\ d_{zz}\ d_{xy}\ d_{xz}\ d_{yz}]^T$ and $\mathbf{a}_i = [x_i^2\ \ y_i^2\ \ z_i^2\ \ 2x_iy_i\ \ 2x_iz_i\ \ 2y_iz_i]^T$.

For $m = 4$ the experiment design is $\mathbf{a}_i = [z_i^4\ 4y_iz_i^3\ 6y_i^2z_i^2\ \ 4y_i^3z_i\ y_i^4\ 4x_iz_i^3\ \ 12x_iy_iz_i^2\ 12x_iy_i^2z_i\ 4x_iy_i^3\ \ 6x_i^2z_i^2\ 12x_i^2y_iz_i\ 6x_i^2y_i^2\ \ 4x_i^3z_i\ 4x_i^3y_i\ x_i^4]^T$.

Note that $d(\mathbf{g},\mathbf{t},m) = d(\mathbf{g})$ is used for simplification. Given measurements in $N > n$ different directions $\mathbf{g}_i$, the least squares estimator of even-order DT is:

$$\hat{\mathbf{t}} = (\mathbf{B}^T\mathbf{B})^{-1}\mathbf{B}^T\mathbf{s}. \tag{2.16}$$

where $\mathbf{B}$ is an $N \times n$ matrix as $\mathbf{B} = [\mathbf{a}_1\ \ \mathbf{a}_2\ \ \cdots\ \mathbf{a}_N]^T$ and $\mathbf{s}$ is a column vector of size N, whose elements are the measured ADC values; i.e. $\mathbf{s} = -\frac{1}{b}[\ln(S_1/S_0)\cdots \ln(S_N/S_0)]^T$. For relatively big N, it is assumed that $\mathbf{B}$ has row rank n. For other HOT estimation approaches see [85, 86]. Unlike the 2nd order DT there is no unified framework for interpretation of high order DTs. In other words, standard definitions of FA and PDD for these models are not immediately obvious. In [79] a framework for the interpretation of HOTs is presented based on the concept of Z-eigenvalues [87] (a generalization of eigen-decomposition to HOTs). An expression for computing the FA from a HOT is also given while [85] proffers an alternative definition.

The only study on GES design for HOTs [27] is limited to comparison of existing GESs mainly devised for second order tensor imaging; e.g. the minimum condition number (MCN) scheme [47]. A caveat here is that the condition number is computed from the design matrix associated with the linear least squares estimation of parameters of interest. Thus, by definition, it is model-dependent. One of the problems considered in this thesis is to find K-optimal and D-optimal GES designs for HOTs.

2.5.4 Diffusion Kurtosis Imaging (DKI)

In order to quantify micro-structural properties of imaged tissues, a wide variety of models have been fitted to the diffusion attenuated MR signal. Of special interest is diffusion kurtosis imaging (DKI) [16, 17] that was proposed to probe the non-Gaussian diffusion. DKI provides biomarkers reflecting pathological and developmental changes in the human brain [88, 89, 90, 91].

The diffusion profile at each voxel is described by two symmetric tensors, a 2nd order diffusion tensor $\mathbf{D}$ (3×3 matrix) and a 4th order kurtosis tensor $\mathbf{W}$ ($3\times 3\times 3\times 3$ matrix). The model that relates the measurements to the unknown parameters is [92]

$$\ln\frac{S(\mathbf{g},b)}{S_0} = -b\sum_{i=1}^{3}\sum_{j=1}^{3} D_{ij}g_ig_j + \frac{1}{6}b^2\bar{D}^2\sum_{i=1}^{3}\sum_{j=1}^{3}\sum_{k=1}^{3}\sum_{l=1}^{3} W_{ijkl}g_ig_jg_kg_l \qquad (2.17)$$

where $\bar{D}=\frac{1}{3}trace(\mathbf{D})$. This model holds under certain conditions, most restrictive of which is the maximum limit for b-value. At least two-shell acquisition is required for DKI model fitting. For more details see [92, 17]. The task in DKI is to estimate 6 distinct elements of $\mathbf{D}$ (denoted by d_{11} to d_{33}) and 15 distinct elements of $\mathbf{W}$ (denoted by w_1 to w_{15}). The model can be reformulated as follows [92]:

$$\ln\frac{S(\mathbf{g}_i,b_j)}{S_0} = \mathbf{a}(i,j)^T\theta \qquad (2.18)$$

where $S(\mathbf{g}_i,b_j)$ is the signal intensity measured in the gradient encoding direction $\mathbf{g}_i=[x_i\ y_i\ z_i]^T$ with diffusion weighting factor b_j and S_0 is the signal intensity with $b_j=0$. The vector of unknown parameters is $\theta=[d_{11}\ d_{22}\ d_{33}\ \ d_{12}\ d_{13}\ d_{23}\ v_1\ v_2\ \cdots\ v_{15}]^T$ where $v_k=\bar{D}^2w_k$. The experiment design is $\mathbf{a}(i,j)=[-b_jx_i^2\ \ -b_jy_i^2\ \ -b_jz_i^2\ \ -2b_jx_iy_i\ \ -2b_jx_iz_i\ \ -2b_jy_iz_i\ \ \frac{b_j^2}{6}x_i^4\ \ \frac{b_j^2}{6}y_i^4\ \ \frac{b_j^2}{6}z_i^4\ \ \frac{2b_j^2}{3}x_iy_i^3\ \ \frac{2b_j^2}{3}x_iz_i^3\ \ \frac{2b_j^2}{3}x_i^3y_i\ \ \frac{2b_j^2}{3}x_i^3z_i\ \ \frac{2b_j^2}{3}y_iz_i^3\ \ \frac{2b_j^2}{3}y_i^3z_i\ \ b_j^2x_i^2y_i^2\ \ b_j^2x^2z^2\ \ b_j^2y_j^2z_j^2\ \ 2b_j^2x_iy_iz_i^2\ \ 2b_j^2x_iy_i^2z_i\ \ 2b_j^2x_i^2y_iz_i]^T$. Given a set of measurements using n non-zero b-values and N_j directions per shell, $\{S(\mathbf{g}_i,b_j)|i=1,\cdots,N_j;j=1,\cdots,n;n\geq 2\}$, the LSE of the unknown parameters is

$$\hat{\theta}=(\mathbf{B}^T\mathbf{B})^{-1}\mathbf{B}^T\mathbf{s}. \qquad (2.19)$$

where the design matrix of size $N\times 21$ is $\mathbf{B}=[\mathbf{a}(1,1)\ \ \mathbf{a}(2,1)\ \ \cdots\ \mathbf{a}(N_n,n)]^T$ and $N=\sum_{j=1}^{n}N_j$, and $\mathbf{s}=[\ln(\frac{S(\mathbf{g}_1,b_1)}{S_0})\ \ \ln(\frac{S(\mathbf{g}_2,b_1)}{S_0})\ \ \cdots\ \ \ln(\frac{S(\mathbf{g}_{N_n},b_n)}{S_0})]$.

2.5.5 Apparent Diffusion Coefficient Imaging

Among the many complicated diffusion models there exist a simple model, i.e. ADC imaging, that is widely used for the classification of brain disorders [93],

detection of malignant breast lesions [94], identifying stages of cerebral infarction [95] and diagnostic imaging of the kidney [96, 97], prostate [98, 99] and ovaries [100, 101]. ADC imaging is also used to solve challenging clinical problems such as differentiation of Parkinson's disease from multiple system atrophy and progressive supranuclear palsy [102].

In essence, ADC imaging is a mono-exponential model fitting problem. The model for ADC imaging is given by

$$S = S_0 \exp(-bD) \tag{2.20}$$

where S is the measured signal when the diffusion weighting factor b is applied, S_0 is the observed signal in the absence of such a weighting factor and D is the apparent diffusion coefficient. The parameters to be estimated are S_0 and D. In ADC imaging the parameter of interest is D (the ADC value).

The popularity of ADC imaging as a quantitative imaging tool has motivated many studies investigating the reliability and reproducibility of ADC estimates [103, 104, 96]. In the case of ADC imaging, an experiment design consists of the b-values applied for measurements and their repetitions. An intuitively appealing experiment design is the equidistant (ED) distribution of sampling points on a valid range of the independent variable (b-values). The range of valid sampling points is determined by the biophysical aspects of the problem at hand. For instance, perfusion contamination at low b-values [105, 104] and SNR drop at high b-values [106] limit the applicable range of b-values. The ED experiment design method is widely used in the literature [107, 96, 108, 109]. However, many studies use non-systematic experiment designs [98, 110] that can considerably influence the results.

Some studies have developed a theoretical framework by minimizing the variance of the estimated parameters [111, 112, 113]. In these studies, the Cramer-Rao lower bound (CRLB) of the ADC value is minimized assuming a Gaussian noise distribution. Hereinafter, we call this method GCRLB. The result of GCRLB is dependent on the range of ADC values to be imaged and the validity of noise assumptions. In this thesis, a new D-optimal experiment design is proposed that partly resolves these problems.

2.6 Applications of dMRI

Once the reconstruction step is done, depending on the model under consideration, a number of features/scalars/vectors the describing underlying tissue characteristics becomes available to be used in the downstream applications. The applications of dMRI (in brain imaging) mainly fall in to two groups: (a) detection of

disease-associated WM changes (based on quantitative diffusion features) and (b) tractography-based diagnosis, surgical planning, etc. Tractography (combining local micro-structure information to obtain neural pathways connecting different parts of the gray matter), is an active research area, playing a key role in the human connectomics. Connectomics is the study of the connectivity in the brain [114]. The dMRI technique provides a structural connectome of the WM.

Developing accurate and robust approaches to describe local diffusion patterns and thereof local micro-structures, is a crucial step in the dMRI processing pipeline. This local micro-structural information is integrated to provide neural pathways inside human brain. The task of reconstructing WM fiber pathways is called tractography and provides a powerful tool to study neuroanatomy of the human brain. Tractography is commonly used for pre-surgical planning in clinics as the only non-invasive way to probe the neural architecture of the human brain in vivo [52]. It is an input to brain structural connectome mapping and brain network analysis.

Two strategies have been taken for tractography: global and local. The local tractography methods fall into two groups: deterministic and probabilistic. They build the pathways based on the information provided by local diffusion patterns. Deterministic tractography starts from a given point (seed) and follows the PDD from one voxel to another. This is terminated if the algorithm reaches the specified destination seed or the fiber runs into low FA regions (that are not supposed to have oriented micro-structures). Positioning way-point seeds is the usual way of improving/regularizing these algorithms. The whole diffusion process and micro-structure estimation in turn, are based on probability theory. Deterministic tractography ignores the uncertainty inherent in the local models of diffusion. One might be interested in the probability of the existence of point-to-point connections, in a more realistic perspective. This has led to probabilistic tractography methods.

In contrast to local tractography, global tractography (GT) considers each path as a parameter to be optimized. The optimality can be defined with respect to different objective functions. Generally, an objective function should in some way measure the diffusion signal fit and concordance with the prior knowledge. The main drawback with GT is its high computational burden. There has been a concerted effort to overcome this drawback [115, 116, 117, 118].

Tractography-related studies are categorized into several groups: (i) studies that aim to estimate fiber orientation distribution functions (fODFs) as accurately as possible [119, 120, 80, 121] (fODFs are the input to any local tractography methods); (ii) studies that introduce new deterministic tractography methods [122, 121, 123, 124, 125, 126]; (iii) studies that introduce new probabilistic tractography methods [121, 127, 124, 125]; (iv) studies that investigate global tractography (in contrast to local tractography) [128, 115, 116, 117, 118]; (v) studies that provide

a review or comparison of different tractography methods and their applications [129, 130, 131]; and (vi) studies based on connectome analysis [132, 116, 114]. This thesis does not include contributions to this part of dMRI analysis. However, the proposed optimal GESs improve the robustness of the information input to this step.

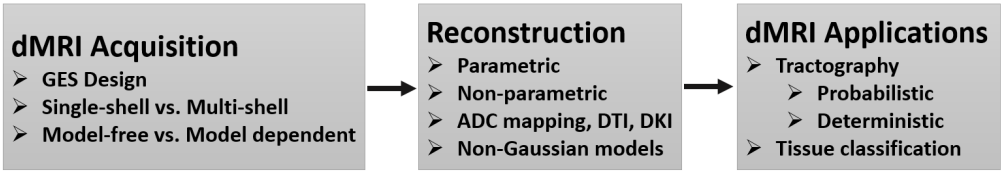

Figure 2.7: Diffusion MRI: Three main steps and corresponding terminology.

To summarize this chapter, the three main steps of diffusion imaging and related terminology are shown in Figure 2.7. The first step is data acquisition where one has to select a gradient encoding scheme (GES) among many other acquisition settings. In the second step, namely reconstruction, acquired data is processed and the underlying micro-structure is characterized using parametric or non-parametric models. A diffusion model can be as simple as the mono-exponential decay (in the case of ADC imaging). However, more advanced models such as 4th order tensors or DKI are required to more thoroughly characterize tissue alteration or complicated micro-structures. In the last step, the collective information is used for tractography or differentiating tissue types.

CHAPTER 3

Summary of the Thesis Work

This chapter briefly describes the work carried out in this thesis. First, in the next section we introduce the problems under consideration and compare experiment design problems in dMRI with some general experiment design problems. Then we summarize the content of the appended papers in separate subsections where we highlight our contributions and present the main results.

3.1 Experiment Design in dMRI: Challenges and New Solutions

Numerous diffusion models have been developed over the last two decades. These models are used to characterise properties of the micro-structures in living tissues. Model fitting is complicated by the fact that the dMRI measurements are inherently noisy (a side effect of MRI signal acquisition). Diffusion parameters find application in medical diagnosis/prognosis. This motivates the investigation of the robustness, reproducibility and reliability of these parameters. One way to achieve robust estimates of diffusion parameters is to optimize the data acquisition setting such that it minimizes the variance of the estimated parameters. This is an optimal experiment design problem (EDP). In the case of ADC imaging, the task is to find the set of applied b-values while for DTI and DKI it involves the design/specification of a GES. In this thesis several EDPs are considered including optimal experiment design for ADC imaging, diffusion tensor imaging (second and fourth order) and diffusion kurtosis imaging.

To better describe the problems at hand, two examples of experiment design

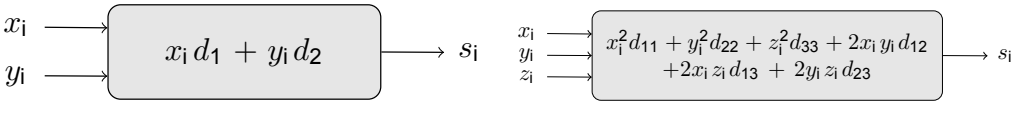

(a) (b)

Figure 3.1: Two examples of the problem in (2.8): (a) Hypothetical experiment design problem with $\theta = [d_1\ d_2]$ and $\mathbf{a}_i = [x_i\ y_i]$. (b) Experiment design problem in second order DTI with $\theta = [d_{11}\ d_{22}\ d_{33}\ d_{12}\ d_{13}\ d_{23}]$ and $\mathbf{a}_i = [x_i^2\ \ y_i^2\ \ z_i^2\ \ 2x_iy_i\ \ 2x_iz_i\ \ 2y_iz_i]^T$.

problems (EDPs) that satisfy (2.8) are presented in Figure 3.1. Figure 3.1-(a) shows a hypothetical experiment design problem with $\theta = [d_1\ d_2]$ and $\mathbf{a}_i = [x_i\ y_i]$. Figure 3.1-(b) describes the experiment design problem in second order DTI with $\theta = [d_{11}\ d_{22}\ d_{33}\ d_{12}\ d_{13}\ d_{23}]$ and $\mathbf{a}_i = [x_i^2\ \ y_i^2\ \ z_i^2\ \ 2x_iy_i\ \ 2x_iz_i\ \ 2y_iz_i]^T$. Both problems are compatible with the formulation in (2.8) although there are key differences. These differences complicate the EDP in several ways including:

- The condition number of the problem in Figure 3.1-(a) can be minimized down to one (the ultimate minimum) while this is not possible in the presence of cross-terms (such as x_iy_i) in the problem in Figure 3.1-(b); and
- For the problem in Figure 3.1-(a), the number of free design parameters (decision variables) for each measurement (two) is equal to the dimension of the design vector $\mathbf{a}_i$ while the number of free design variables for DTI is less than the dimension of the design vector.

The EDPs in this thesis cannot be solved by straight forward application of approaches in the optimization literature for the following reasons:

- The problems under consideration in this thesis, unlike problems in [133, 19, 18], are not convex; and
- The conventional experiment design problems (as in [18]) seek to minimize the objective function over a finite and thus countable set $\mathscr{A}$, i.e. $\forall i : \mathbf{a}_i \in \mathscr{A}$. In this thesis, however, $\mathscr{A}$ is not a countable set but includes the whole set of feasible solutions.

The general formulation for GES design problems in this thesis is as follows:

$$\begin{aligned} &\min_{\mathbf{g}_i}\ \ \mathscr{F}(\mathbf{M}^{-1}) \\ &\text{s.t.}:\ \ \mathbf{M} \geq 0, \quad ||\mathbf{g}_i|| = 1, i = 1, \cdots, N. \end{aligned} \tag{3.1}$$

where $\mathscr{F} : \mathbb{R}^{n\times n} \to \mathbb{R}$ is a scalarization function (such as the trace, determinant, condition number), n is the size of the information matrix $\mathbf{M}$ and the $\mathbf{g}_i$s are the

gradient encoding directions. The size of the information matrix depends on the model under consideration. It is listed for even order DTI, DKI and ADC imaging in Table 3.1. It is noteworthy that in experiment design for ADC imaging, decision variables are b_is instead of $\mathbf{g}_i$s (thus the constraints on $\mathbf{g}_i$ in (3.1) should be replaced with $b_{min} \leq b_i \leq b_{max}$). The problem above is not convex. However, it can be converted to a convex problem and solved by semi-definite programming.

Table 3.1: Dimension of the information matrix (n) in optimal experiment design problems of dMRI

Model	DTI2	DTI4	DTI6	DKI	ADC
n	6	15	28	21	2

There exists a set of studies considering the same EDPs as this thesis. The proposed method differs from the previous studies in several respects. In contrast to [35, 47], it does not utilize stochastic optimization techniques. It does not involve any simplification/discretization of the original problem as in [34, 35]. Unlike [35, 34, 47], it provides theoretical and practical properties of the obtained solutions. In comparison to [28], it produces (exactly) rotation-invariant gradient encoding schemes (in the case of D-optimal design). Finally, it establishes a general theoretical framework for GES design in dMRI by extending the proposed method to modern diffusion imaging techniques (e.g. HOTs and DKI).

In following sections, a summary of our findings for each model is presented.

3.2 Second Order DTI

The problem of GES design for 2nd order DTI is considered in *Papers A, E* and *F*. The icosahedral scheme is well-known in the dMRI literature. However, a simple algorithm to generate the icosahedral scheme for an arbitrary number of measurements does not exist. In *Paper E*, such an algorithm is proposed. The algorithm generates the exact (with the condition number of 1.5811) and rotation-invariant GESs although they are not necessarily UD.

In *Paper F*, a simple algorithm for the computation of the K-optimal GES for second order DTI is proposed. The algorithm: (i) does not need stochastic optimization; (ii) reveals several theoretical properties of K-optimal designs; and (iii) works for an arbitrary number of measurements. Both *Papers E* and *F*, were based on conjectures giving the optimal information matrix. Later, in *Paper A*, all these findings are proved and formulated under a unified framework.

The unified approach to find analytical solutions for A,E,K,D-optimal experiment design problems for second order DTI is developed in *Paper A*. The infor-

mation matrix (**M** in (3.1)) for 2nd order DTI is

$$\mathbf{M} = \begin{bmatrix} \sum x_i^4 & \sum x_i^2 y_i^2 & \sum x_i^2 z_i^2 & 2\sum x_i^3 y_i & 2\sum x_i^3 z_i & 2\sum x_i^2 y_i z_i \\ \sum x_i^2 y_i^2 & \sum y_i^4 & \sum y_i^2 z_i^2 & 2\sum y_i^3 x_i & 2\sum y_i^2 x_i z_i & 2\sum y_i^3 z_i \\ \sum x_i^2 z_i^2 & \sum y_i^2 z_i^2 & \sum z_i^4 & 2\sum z_i^2 x_i y_i & 2\sum z_i^3 x_i & 2\sum z_i^3 y_i \\ 2\sum x_i^3 y_i & 2\sum y_i^3 x_i & 2\sum z_i^2 x_i y_i & 4\sum x_i^2 y_i^2 & 4\sum x_i^2 y_i z_i & 4\sum y_i^2 x_i z_i \\ 2\sum x_i^3 z_i & 2\sum y_i^2 x_i z_i & 2\sum z_i^3 x_i & 4\sum x_i^2 y_i z_i & 4\sum x_i^2 z_i^2 & 4\sum z_i^2 x_i y_i \\ 2\sum x_i^2 y_i z_i & 2\sum y_i^3 z_i & 2\sum z_i^3 y_i & 4\sum y_i^2 x_i z_i & 4\sum z_i^2 x_i y_i & 4\sum y_i^2 z_i^2 \end{bmatrix} \tag{3.2}$$

Our proposed solution involves the following steps:

- Change decision/design variables, i.e. obtain optimal moments (e.g. $\sum x_i^4$) instead of optimal directions (e.g. $[x_i\ y_i\ z_i]$). This reduces the number of design variables (from $3N$ to 15, in the case 2nd order DTI).
- Convert N non-convex constraints to one convex constraint as follows. The non-convex constraints imply that $\sum_{i=1}^{N} ||\mathbf{g}_i||^4 = N$. This is a convex constraint on new decision variables (convex relaxation).
- Solve the resulting semi-definite programming problem.
- Recover/retrieve the original design variables (gradient encoding directions).

A summary of results follows. Common to all types of optimal designs (A/E/K/D), odd moments must be zero (e.g. $\sum x_i^3 y_i = \sum x_i^2 y_i z_i = 0$). In the case of K-optimal and E-optimal design, even moments are:

$$\begin{array}{l} \sum x_i^4 = \sum y_i^4 = \sum z_i^4 = \frac{5N}{21}, \\ \sum x_i^2 y_i^2 = \sum x_i^2 z_i^2 = \sum z_i^2 y_i^2 = \frac{N}{21}. \end{array} \tag{3.3}$$

The D-optimal design requires the even moments to satisfy the following conditions:

$$\begin{array}{l} \sum x_i^4 = \sum y_i^4 = \sum z_i^4 = \frac{3N}{15}, \\ \sum x_i^2 y_i^2 = \sum x_i^2 z_i^2 = \sum z_i^2 y_i^2 = \frac{N}{15}. \end{array} \tag{3.4}$$

The A-optimal design requires the even moments to satisfy the following conditions:

$$\begin{array}{l} \sum x_i^4 = \sum y_i^4 = \sum z_i^4 = \frac{N}{4.5672}, \\ \sum x_i^2 y_i^2 = \sum x_i^2 z_i^2 = \sum z_i^2 y_i^2 = \frac{N}{17.4853}. \end{array} \tag{3.5}$$

Further study/evaluation of the proposed GESs, yields the following insights/conclusions for second order tensors:

- The traditionally used icosahedral scheme is a subset of D-optimal designs.

- The D-optimal design is rotation-invariant with respect to all four (A/E/K/D) optimality metrics. (See the proof in Section 3.8.1).
- The proposed method can be used to compute the optimal design for an arbitrary number of measurements. In Figure 3.2-(a), N=11 is deliberately chosen to highlight this property.
- The determinant of the information matrix is a rotation invariant optimality metric.
- For N=6, the D-optimal design reproduces the icosahedral scheme (see Table 3.2). However, the D-optimal design generates GESs that deviate from uniformity for large values of N (see Figure 2.4).
- One can re-run the proposed algorithm to find uniformly distributed D-optimal solutions. For example, the solutions with the largest β_{min} among 1000 runs for N=11, 15, 20 and 30 are shown in Figure 3.2.

Table 3.2: D-Optimal GES design reproduces the well-known icosahedral scheme [47, 32] for $N = 6$ with $\beta_{min} = \beta_{max} = 63.4349^\circ$. However, these exist non-UD D-optimal solutions for large values of N.

x_i	y_i	z_i
-0.0421	0.3135	-0.9487
0.1214	0.9808	-0.1527
-0.3864	0.6113	0.6906
0.8149	-0.5156	0.2648
0.8639	0.2843	-0.4158
0.6511	0.4684	0.5973

Our Monte-Carlo simulations (Table 3.3) show that the D-optimal design leads to the minimum variance estimation of the diffusion parameters. Thus, we conclude that the D-optimal design is the most useful method for GES design of 2nd order tensors (because of rotation-invariance, UD solutions and minimum variance estimation of diffusion parameters).

Among existing methods, the ER scheme [28] is the most popular one. As can be seen in Table 3.3, the difference between the ER scheme and the D-optimal scheme is negligible for 2nd order DTI. However, as shown in *Paper A*, it is well-pronounced for high order models. In addition, the possibility of extensions to GES design for high order tensors is demonstrated in *paper A*. Another important theoretical contribution of *Paper A* is that it provides the first mathematical proof of optimality of UD GESs.

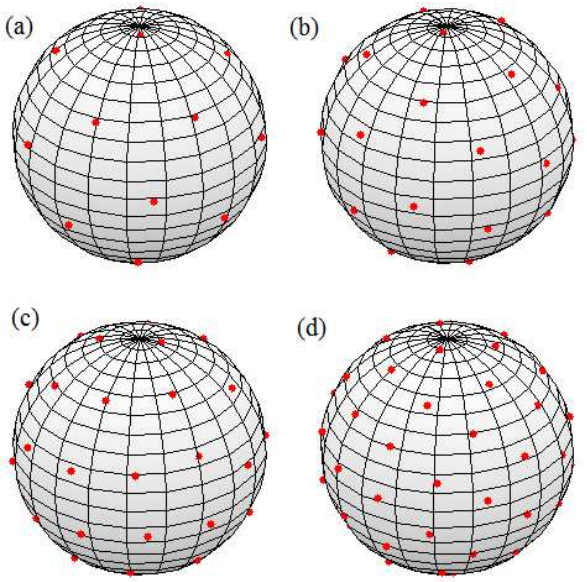

Figure 3.2: The D-optimal design with the largest β_{min} among 1000 runs for (a) N=11, β_{min} =41.1°; (b) N=15, β_{min} =31.9°; (c) N=20, β_{min} =29.3°; and (d) N=30, β_{min} =24.0°.

Table 3.3: Statistics of the robustness test performed according to Algorithm 1 given in the previous Chapter ($N = 20$). The ER scheme is proposed in [41, 28]. The parameter, CU_{95} is defined in [61] to quantify the uncertainty in the estimation of PDD

Scheme	Mean(σ(FA))	Std(σ(FA))	Mean(CU_{95})°	Std(CU_{95})	β_{min}°
D-opt	0.0480	0.0013	9.98	0.28	29.3
ER	0.0482	0.0013	9.98	0.30	28.8
K-opt	0.0492	0.0069	10.88	1.19	9.7

3.3 Fourth Order DTI

The problem of GES design for 4th order DTI is considered in *Paper B*. The optimal GES design approach that was originally developed for second order DTI (in *Paper A*) is extended to fourth order DT estimation. In particular, *Paper B* proposes K-optimal design for fourth order DTI. Comparisons with previous work and theoretical results are also presented in this paper. In addition, part of *Paper A* is devoted to solving D-optimal GES design for fourth order DTI. In the proposed method (*Paper B*), the K-optimal design problem for fourth order DTI is

formulated as an SDP problem:

$$\begin{aligned} &\min_{\mathbf{q},p} \ \alpha \\ &\text{s.t.}: \ \mathbf{M}(\mathbf{q}) \geq 0, \ \mathbf{I} \leq p\mathbf{M}(\mathbf{q}) \leq \alpha\mathbf{I} \\ &\quad p \geq 0, \ \mathbf{u}^T\mathbf{q} = N. \end{aligned} \tag{3.6}$$

where $\mathbf{M}$ is the information matrix, $\mathbf{I}$ is the identity matrix, α is the condition number of $\mathbf{M}$, $\mathbf{q} \in \mathbb{R}^{45}$ includes the moments of a GES (for example, $q_1 = \sum x_i^8$ and $q_{10} = \sum x_i^4 y_i^4$), $\mathbf{u} \in \mathbb{R}^{45}$ is constant vector with only fifteen non-zero elements, and p equals $1/\lambda_{min}(\mathbf{M})$ (λ_{min} denotes the minimum eigenvalue). The optimal value α^* in (3.6) is obtained by performing a line search on p. Let the optimal value of the following problem be α_c^* where c is a real non-negative constant:

$$\begin{aligned} &\min_{\mathbf{q}} \ \alpha \\ &\text{s.t.}: \ \mathbf{M}(\mathbf{q}) \geq 0, \ \mathbf{I} \leq c\mathbf{M}(\mathbf{q}) \leq \alpha\mathbf{I}, \ \mathbf{u}^T\mathbf{q} = N \end{aligned} \tag{3.7}$$

Then $\alpha^* = \min\{\alpha_c^* | c \in \mathbb{R}_+\}$. Details on variable change, convex relaxation and the extraction of the original variables from the optimal information matrix can be found in *Paper B*.

Using the same notation/strategy, the D-optimal design problem for fourth order DTI is formulated as an SDP problem (*Papers A and C*):

$$\begin{aligned} &\min_{\mathbf{q}} \quad -\log\det(\mathbf{M}) \\ &\text{s.t.}: \ \mathbf{M}(\mathbf{q}) \geq 0, \ \mathbf{u}^T\mathbf{q} = N. \end{aligned} \tag{3.8}$$

The problems in (3.7) and (3.8) can be efficiently solved by LMI solvers. In summary, our findings concerning fourth order DT estimation include:

- The D-optimal GES is rotation-invariant (See the proof in Section 3.8.2).
- The D-optimal design for the fourth order tensor is also D-optimal for the 2nd order tensor, however, the converse is not true (See the proof in Section 3.5).
- The D-optimal design for fourth order tensors yields GESs with uniform coverage of the unit sphere, for a practical range of N.
- The icosahedral scheme is D-optimal for fourth order tensor estimation.
- The proposed method can be used to compute the D/K-optimal design for an arbitrary number of measurements.
- The odd moments of the K-optimal design are zero.

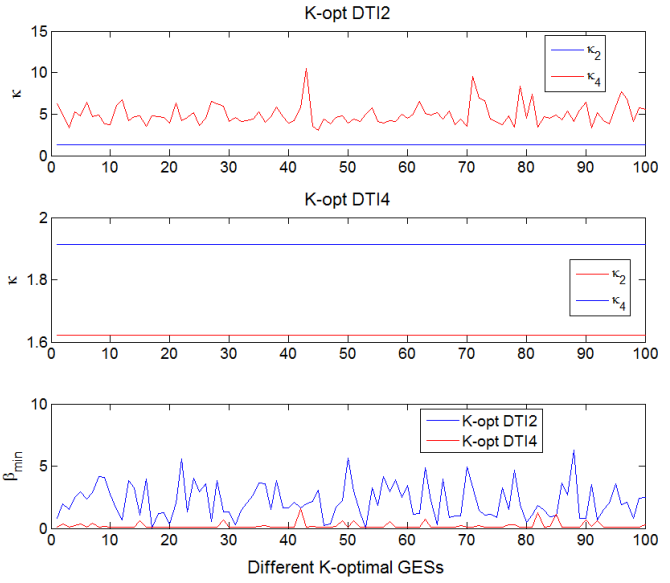

Figure 3.3: A comparison of the K-optimal GESs for 100 runs of the proposed algorithm: 2nd and 4th order DTI are denoted by DTI2 and DTI4, respectively. The condition numbers of the 2nd and 4th order information matrices are shown by κ_2 and κ_4, respectively ($N = 30$).

- The even moments of the K-optimal design are proportional to the total number of measurements.
- The K-optimal design is not unique, in general (See the proof in *Paper B*).
- The D-optimal design is not unique.

A previous study [27] compared existing GESs for 4th order DTI. This study emphasizes that the numerically optimized schemes (e.g. ER and MCN) vary with each optimization. *Paper B* represents a clear advancement by solving the K-optimal design problem and describing the relationship between different solutions. Solutions of the K-optimal design problem (both 2nd and 4th order DTI) for 100 runs of the proposed algorithm are compared in Figure 3.3. It can be seen that: (i) the proposed algorithm consistently provides the optimal solution for both 2nd and 4th order DTI; (ii) the K-optimal GES for 2nd order DTI is sub-optimal for 4th order DTI; (iii) the K-optimal GES for 4th order DTI is sub-optimal for 2nd order DTI. Consequently, one should not use the same GES as the K-optimal design for both 2nd and 4th order DTI (as was done in [27]); and (iv) the K-optimal designs for both 2nd and 4th order DTI are also different in terms of the uniformity of distribution of gradient encoding directions.

3.4 Diffusion Kurtosis Imaging (DKI)

The extension of the proposed method to non-Gaussian/modern diffusion models that require multi-shell acquisitions (such as DKI) significantly enhances the theory/approach developed in this thesis. DKI is a technique that can provide biomarkers reflecting pathological and developmental changes in the human bran [88, 89, 90, 91]. Motivated by this fact, an optimal experiment design method for DKI is given in *Paper C*.

In *Paper C*, the D-optimal design problem for DKI is converted to the following convex optimization problem:

$$\begin{array}{l} \min_{\mathbf{p}} \ \ -\log\det(\mathbf{M}(\mathbf{p})) \\ \text{s.t.}: \ \ \mathbf{M}(\mathbf{p}) \geq 0, \quad \mathbf{u}^T\mathbf{q} = N_1,\ \mathbf{u}^T\mathbf{q}' = N_2, \\ \mathbf{r}^T\mathbf{q} = N_1,\ \mathbf{r}^T\mathbf{q}' = N_2,\ \mathbf{t}^T\mathbf{q} = N_1,\ \mathbf{t}^T\mathbf{q}' = N_2 \end{array} \tag{3.9}$$

where $\mathbf{r}$, $\mathbf{t}$ and $\mathbf{u}$ are some suitable constant vectors in $\mathbb{R}^{88}$, $\mathbf{q}$ and $\mathbf{q}'$ are vectors containg moments of a GES for the first and second shell, respectively, N_1 and N_2 are the number of points on the first and second shell, and $\mathbf{p} \in \mathbb{R}^{176}$ (consists of the variables in $\mathbf{q}$ and $\mathbf{q}'$). The solution to this problem described in *Paper C*, leads us to the following major findings:

- The conventional icosahedral scheme is approximately D-optimal for DKI.
- The proposed D-optimal design is rotation-invariant. (See the proof in sections 3.8.1 and 3.8.2).
- There exists a D-optimal solution for DKI which is simultaneously D-optimal for 2nd and 4th order diffusion tensor estimation.
- The proposed method can be used to compute the optimal design for an arbitrary number of measurements and shells.
- D-optimality enforces the uniform distribution of gradient encoding directions for a typical number of measurements in DKI.
- The solution of the DKI D-optimal design problem is not unique.
- The proposed method optimizes both gradient encoding directions and *b*-values.

The work in *Paper C* establishes a theoretical foundation for the experiment design in other diffusion imaging techniques that utilize linear models. Importantly, these theoretical findings provide the first mathematical proof of the optimality of uniformly distributed GESs for DKI.

3.5 Model-independent GES Design

From the material presented in *Papers A, C, E* and *F*, it can be seen that it is possible to find a set of solutions that are D-optimal for several diffusion models at the same time. This set includes UD schemes (e.g. the icosahedral scheme). Given that the UD schemes are widely used for diffusion imaging (irrespective of the diffusion model under consideration), the proposed method can be regarded as a model-independent GES design method. In other words, it can be used for other diffusion imaging techniques as well.

The D-optimal GES for a high order model is also D-optimal for all lower order models. For example, there exist a DKI D-optimal design that is simultaneously D-optimal for second and fourth order DTI, as well. This is discussed in *Paper C*. In addition, D-optimal design for fourth order DTI is simultaneously D-optimal for DKI and second order DTI (See the proof below). This enhances the practical impact of the proposed method and extends its utility beyond the model under consideration (although the proposed method is model-dependent by construction).

Here, we prove that the D-optimal design for fourth order DTI is also D-optimal for second order DTI and DKI. The D-optimal design for the fourth order tensor is given by the following equations (obtained in *Paper A*):

$$\begin{aligned}
&\textstyle\sum x_i^8 = \sum y_i^8 = \sum z_i^8 = \frac{N}{9} \\
&\textstyle\sum x_i^2 y_i^6 = \sum x_i^6 y_i^2 = \sum x_i^2 z_i^6 = \sum x_i^6 z_i^2 = \sum z_i^2 y_i^6 = \sum z_i^6 y_i^2 = \frac{N}{63} \\
&\textstyle\sum x_i^4 y_i^4 = \sum x_i^4 z_i^4 = \sum z_i^4 y_i^4 = \frac{N}{105} \\
&\textstyle\sum y_i^4 x_i^2 z_i^2 = \sum z_i^4 x_i^2 y_i^2 = \sum x_i^4 y_i^2 z_i^2 = \frac{N}{315}
\end{aligned} \tag{3.10}$$

The task is to compute values of all design moments required for DKI (4th-,6th- and 8th-order moments). The 8th order moments are already known from the definition of D-optimality for fourth order DTI. Thus, we need to show that 4th and 6th order moments also take the DKI D-optimal values given in *Paper C*. Let us start by computing 6th order moments. Given that $x_i^2 + y_i^2 + z_i^2 = 1$, we multiply this equation by x_i^6 yielding:

$$\begin{aligned}
&x_i^8 + x_i^6 y_i^2 + x_i^6 z_i^2 = x_i^6 \Rightarrow \textstyle\sum x_i^8 + \sum x_i^6 y_i^2 + \sum x_i^6 z_i^2 = \sum x_i^6 \\
&\Rightarrow \textstyle\sum x_i^6 = \frac{N}{9} + \frac{2N}{63} = \frac{N}{7}
\end{aligned} \tag{3.11}$$

Similarly one can compute all 6th degree moments of the design. They all take

the DKI D-optimal values:

$$\begin{array}{l}\sum x_i^6 = \sum y_i^6 = \sum z_i^6 = \frac{N}{7} \\ \sum x_i^2 y_i^4 = \sum x_i^2 z_i^4 = \sum x_i^4 y_i^2 = \sum x_i^4 z_i^2 = \sum z_i^2 y_i^4 = \sum z_i^4 y_i^2 = \frac{N}{35} \\ \sum x_i^2 y_i^2 z_i^2 = \frac{N}{105}\end{array} \tag{3.12}$$

Knowing the 6th degree moments, one can proceed with the computation of the 4th degree moments:

$$\begin{array}{l} x_i^2 + y_i^2 + z_i^2 = 1 \Rightarrow x_i^6 + x_i^4 y_i^2 + x_i^4 z_i^2 = x_i^4 \\ \Rightarrow \sum x_i^6 + \sum x_i^4 y_i^2 + \sum x_i^4 z_i^2 = \sum x_i^4 \Rightarrow \sum x_i^4 = \frac{N}{7} + \frac{2N}{35} = \frac{N}{5}\end{array} \tag{3.13}$$

Similarly one can compute all 4th degree moments of the design to see that they take DKI D-optimal values:

$$\begin{array}{l}\sum x_i^4 = \sum y_i^4 = \sum z_i^4 = \frac{N}{5}, \\ \sum x_i^2 y_i^2 = \sum x_i^2 z_i^2 = \sum z_i^2 y_i^2 = \frac{N}{15}\end{array} \tag{3.14}$$

Similarly one can show that all 6th and 4th degree odd moments are equal to zero. Thus, D-optimality for fourth order DTI ensures D-optimality for DKI and second order DTI. It is worth mentioning that the converse is, in general, not true.

3.6 Optimal Design for ADC imaging

The problem of optimal experiment design for ADC imaging is addressed in *Paper D*. ADC imaging is an estimation problem that conforms to (2.8). Its information matrix is:

$$\mathbf{M} = \begin{bmatrix} N & -\sum_{i=1}^N b_i \\ -\sum_{i=1}^N b_i & \sum_{i=1}^N b_i^2 \end{bmatrix} \tag{3.15}$$

where N is the total number of measurements. Noting that minimizing $\det(\mathbf{M}^{-1})$ is equivalent to maximizing $\det(\mathbf{M})$ we need to solve the following problem:

$$\begin{array}{ll}\max & \det(\mathbf{M}) \\ \text{s.t.:} & \mathbf{M} \geq 0, \;\; b_{min} \leq b_i \leq b_{max}, i = 1, \cdots, N.\end{array} \tag{3.16}$$

The explicit form of the objective function is:

$$\det(\mathbf{M}) = N \sum_{i=1}^N b_i^2 - (\sum_{i=1}^N b_i)^2 \tag{3.17}$$

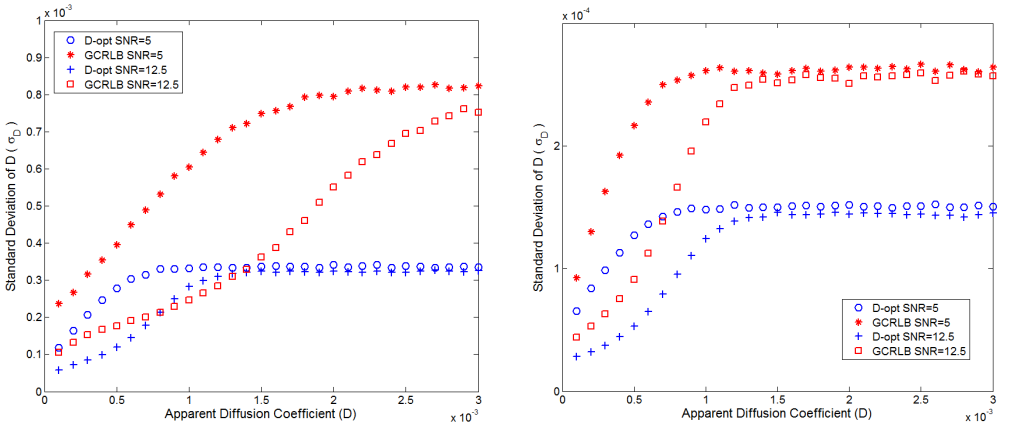

(a) N=2 (b) N=10

Figure 3.4: Standard deviation of the estimated ADC values (σ_D) for a range of D values where $b_{min} = 0$, $b_{max} = 1500$, $S_0 = 500$, $N_{MC} = 20000$ (number of Monte Carlo trials) and SNR=S_0/σ_G (Rician distributed noise). The proposed D-optimal method is compared to GCRLB [113].

Thus, one can see that for an arbitrary N, the D-optimal experiment design is:

$$\begin{aligned} b_i &= b_{min} \quad i = 1, \cdots, n \\ b_i &= b_{max} \quad i = n+1, \cdots, N \end{aligned} \tag{3.18}$$

where $n = N/2$ if N is even, otherwise $n = (N+1)/2$. The proposed theoretical framework for the optimal experiment design of mono-exponential model fitting has the following advantages: (i) in comparison to GCRLB [113], it imposes fewer restrictions on the noise distribution; and (ii) in contrast to GCRLB, the proposed design is independent of the imaged parameters. The proposed D-optimal experiment design for ADC imaging is compared to GCRLB [113] in Figure 3.4. It can be seen that the D-optimal design consistently outperforms GCRLB.

3.7 A New Framework for Repeated Measurements in DTI

This section briefly describes the studies presented in *Papers G* and *H*. In experiment design theory, the optimal GES is obtained by minimizing the covariance matrix of the estimated parameters in some sense, as mentioned earlier. In this regard, K-optimal [47] and D-optimal (in *Paper A*) GES design methods have been developed. It is known that the condition number is invariant under repetition [134]. Even the new optimality metrics, such as the determinant of the information matrix are invariant under repetitions (see *Paper A*). The following choices

are equally good (in terms of condition number/determinat): (i) optimizing for N_t unique directions, i.e. $N_u = N_t$; (ii) optimizing for $N_u = N_t/M$ unique directions and repeating measurements M times; and (iii) using a combination of optimized GESs for N_1 and N_2 directions where $N_1 + N_2 = N_t$.

In the diffusion MRI literature, the question of whether given a fixed scan time, it is better to make measurements in all unique directions or to repeat measurements in a smaller number of directions has received considerable attention [134, 135, 136, 137, 138, 3, 139, 31]. Differences in what is meant by a repeated measurement arise as a consequence of where and how noise is accounted for. There are two strategies: to estimate the signal from complex-valued raw data or from real-valued magnitude data. This distinction was first highlighted in [140] where a theoretical analysis for the *maximum likelihood estimation* (MLE) of structural MR images was given. Inspired by [140], we investigate the effect of choosing real or complex-valued data on the estimation of diffusion parameters. Specifically, we propose a new acquisition/processing pipeline based on the second strategy. The lack of ground truth for real data and the intractability of mathematical derivations make it difficult to investigate the effect of the processing pipeline on the robustness of tensor estimation. However, Monte Carlo simulations can shed light on this problem. In *Papers G* and *H*, we have investigated the issue of repeated measurements. The main contributions of these papers are:

- A new approach for acquiring and processing repeated measurements in DTI is presented.
- The new framework improves precision in the estimation of diffusion parameters.
- The new framework allows us to exploit knowledge of the noise distribution to enhance the SNR.

Details can be found in *Papers G* and *H*.

3.8 Appendix

3.8.1 Proof of Rotation-invariance for D-optimal Design for 2nd order DTI

The rotation-invariance property of the proposed D-optimal design for second order DTI is illustrated in *Paper A* using Monte Carlo simulations. The proof of this

property (discussed in Section 3.2) is given here. First, let us define the following notation:

$$\begin{array}{lll} q_1 = \sum x_i^4 & q_2 = \sum y_i^4 & q_3 = \sum z_i^4 \\ q_4 = \sum x_i^2 y_i^2 & q_5 = \sum x_i^2 z_i^2 & q_6 = \sum z_i^2 y_i^2 \\ q_7 = \sum x_i^3 y_i & q_8 = \sum x_i y_i^3 & q_9 = \sum x_i^3 z_i \\ q_{10} = \sum x_i z_i^3 & q_{11} = \sum y_i^3 z_i & q_{12} = \sum y_i z_i^3 \\ q_{13} = \sum x_i^2 y_i z_i & q_{14} = \sum x_i y_i^2 z_i & q_{15} = \sum x_i y_i z_i^2. \end{array} \tag{3.19}$$

Let the moments of the rotated GES be denoted by $q_c^{\mathbf{R}}$. The D-optimal values of the even moments are given in (3.4). The odd moments of D-optimal design are equal to zero. Below, we prove the rotation invariance for q_1.

$$\begin{aligned} & q_1 = \sum x_i^4 = \tfrac{N}{5} \implies q_1^{\mathbf{R}} = \sum (r_{11}x_i + r_{12}y_i + r_{13}z_i)^4 \\ & = q_1 r_{11}^4 + q_2 r_{12}^4 + q_3 r_{13}^4 \\ & + 6(q_4 r_{11}^2 r_{12}^2 + q_6 r_{12}^2 r_{13}^2 + q_5 r_{11}^2 r_{13}^2) \\ & + 12(q_{13} r_{11}^2 r_{12} r_{13} + q_{14} r_{11} r_{12}^2 r_{13} + q_{15} r_{11} r_{12} r_{13}^2) \\ & + 4(q_7 r_{11}^3 r_{12} + q_8 r_{11} r_{12}^3 + q_9 r_{11}^3 r_{13} + q_{10} r_{11} r_{13}^3 \\ & + q_{11} r_{12}^3 r_{13} + q_{12} r_{12} r_{13}^3) \\ & = \tfrac{N}{5}(r_{11}^4 + r_{12}^4 + r_{13}^4) + 6\tfrac{N}{15}(r_{11}^2 r_{12}^2 + r_{12}^2 r_{13}^2 + r_{11}^2 r_{13}^2) \\ & = \tfrac{N}{5}(r_{11}^2 + r_{12}^2 + r_{13}^2)^2 = \tfrac{N}{5}. \end{aligned}$$

In the derivations above, we substitute D-optimal values of the moments and use properties of a rotation matrix. The proof for other moments is similar.

3.8.2 Proof of Rotation-invariance for D-optimal Design for the 4th order DTI

The proof of the rotation invariance of the proposed D-optimal design for fourth order DTI (discussed in Section 3.3) is given below. First, we define the following

notation:

$$
\begin{array}{lll}
q_1 = \sum x_i^8 & q_2 = \sum y_i^8 & q_3 = \sum z_i^8 \\
q_4 = \sum x_i^4 z_i^4 & q_5 = \sum z_i^4 y_i^4 & q_6 = \sum x_i^4 y_i^4 \\
q_7 = \sum x_i^2 y_i^2 z_i^4 & q_8 = \sum x_i^4 y_i^2 z_i^2 & q_9 = \sum x_i^2 y_i^4 z_i^2 \\
q_{10} = \sum z_i^6 y_i^2 & q_{11} = \sum x_i^6 y_i^2 & q_{12} = \sum x_i^2 y_i^6 \\
q_{13} = \sum x_i^6 z_i^2 & q_{14} = \sum x_i^2 z_i^6 & q_{15} = \sum z_i^2 y_i^6 \\
q_{16} = \sum x_i^5 y_i^3 & q_{17} = \sum x_i^3 y_i^5 & q_{18} = \sum z_i^5 x_i^3 \\
q_{19} = \sum z_i^3 x_i^5 & q_{20} = \sum z_i^3 y_i^5 & q_{21} = \sum y_i^3 z_i^5 \\
q_{22} = \sum x_i^7 y_i & q_{23} = \sum x_i y_i^7 & q_{24} = \sum z_i^7 x_i \\
q_{25} = \sum x_i^7 z_i & q_{26} = \sum y_i^7 z_i & q_{27} = \sum y_i z_i^7 \\
q_{28} = \sum x_i^4 y_i^3 z_i & q_{29} = \sum x_i^4 y_i z_i^3 & q_{30} = \sum y_i^4 z_i^3 x_i \\
q_{31} = \sum x_i^3 y_i^4 z_i & q_{32} = \sum x_i^3 z_i^4 y_i & q_{33} = \sum x_i y_i^3 z_i^4 \\
q_{34} = \sum x_i^5 y_i^2 z_i & q_{35} = \sum x_i^5 z_i^2 y_i & q_{36} = \sum y_i^5 z_i^2 x_i \\
q_{37} = \sum x_i^2 z_i y_i^5 & q_{38} = \sum x_i^2 z_i^5 y_i & q_{39} = \sum x_i y_i^2 z_i^5 \\
q_{40} = \sum x_i^6 z_i y_i & q_{41} = \sum x_i y_i^6 z_i & q_{42} = \sum y_i z_i^6 x_i \\
q_{43} = \sum x_i^3 y_i^3 z_i^2 & q_{44} = \sum x_i^3 z_i^3 y_i^2 & q_{45} = \sum x_i^2 y_i^3 z_i^3.
\end{array}
\tag{3.20}
$$

The D-optimal values of even moments are specified in (3.10). All odd moments are equal to zero (for a D-optimal GES). Below, we prove rotation invariance for q_1. Let the moments of the rotated GES be denoted by $q_c^{\mathbf{R}}$. The proof can be obtained as follows:

$$
\begin{aligned}
&q_1 = \sum x_i^8 = \tfrac{N}{9} \implies q_1^{\mathbf{R}} = \sum (r_{11}x_i + r_{12}y_i + r_{13}z_i)^8 \\
&= q_1 r_{11}^8 + q_2 r_{12}^8 + q_3 r_{13}^8 \\
&+70(q_6 r_{11}^4 r_{12}^4 + q_5 r_{12}^4 r_{13}^4 + q_4 r_{11}^4 r_{13}^4) \\
&+56(q_{40} r_{11}^6 r_{12} r_{13} + q_{41} r_{11} r_{12}^6 r_{13} + q_{42} r_{11} r_{12} r_{13}^6) \\
&+8(q_{22} r_{11}^7 r_{12} + q_{23} r_{11} r_{12}^7 + q_{25} r_{11}^7 r_{13} + q_{24} r_{11} r_{13}^7 + q_{26} r_{12}^7 r_{13} + q_{27} r_{12} r_{13}^7) \\
&+28(q_{11} r_{11}^6 r_{12}^2 + q_{12} r_{11}^2 r_{12}^6 + q_{13} r_{11}^6 r_{13}^2 + q_{14} r_{11}^2 r_{13}^6 + q_{15} r_{12}^6 r_{13}^2 + q_{10} r_{12}^2 r_{13}^6) \\
&+56(q_{16} r_{11}^5 r_{12}^3 + q_{17} r_{11}^3 r_{12}^5 + q_{19} r_{11}^5 r_{13}^3 + q_{18} r_{11}^3 r_{13}^5 + q_{20} r_{12}^5 r_{13}^3 + q_{21} r_{12}^3 r_{13}^5) \\
&+168(q_{34} r_{11}^5 r_{12}^2 r_{13} + q_{35} r_{11}^5 r_{12} r_{13}^2 + q_{37} r_{11}^2 r_{12}^5 r_{13} + q_{36} r_{11} r_{12}^5 r_{13}^2 + q_{38} r_{11}^2 r_{12} r_{13}^5 \\
&+q_{39} r_{11} r_{12}^2 r_{13}^5) \\
&+280(q_{28} r_{11}^4 r_{12}^3 r_{13} + q_{29} r_{11}^4 r_{12} r_{13}^3 + q_{31} r_{11}^3 r_{12}^4 r_{13} + q_{30} r_{11} r_{12}^4 r_{13}^3 + q_{32} r_{11}^3 r_{12} r_{13}^4 \\
&+q_{33} r_{11} r_{12}^3 r_{13}^4) \\
&+420(q_8 r_{11}^4 r_{12}^2 r_{13}^2 + q_9 r_{11}^2 r_{12}^4 r_{13}^2 + q_7 r_{11}^2 r_{12}^2 r_{13}^4) \\
&+560(q_{40} r_{11}^2 r_{12}^3 r_{13}^3 + q_{41} r_{11}^3 r_{12}^2 r_{13}^3 + q_{42} r_{11}^3 r_{12}^3 r_{13}^2) \\
&= \tfrac{N}{9}(r_{11}^8 + r_{12}^4 + r_{13}^8) + 70\tfrac{N}{105}(r_{11}^4 r_{12}^4 + r_{12}^4 r_{13}^4 + r_{11}^4 r_{13}^4) \\
&+28\tfrac{N}{63}(r_{11}^6 r_{12}^2 + r_{11}^2 r_{12}^6 + r_{11}^6 r_{13}^2 + r_{11}^2 r_{13}^6 + r_{12}^6 r_{13}^2 + r_{12}^2 r_{13}^6) \\
&+420\tfrac{N}{315}(r_{11}^4 r_{12}^2 r_{13}^2 + r_{11}^2 r_{12}^4 r_{13}^2 + r_{11}^2 r_{12}^2 r_{13}^4) \\
&= \tfrac{N}{9}(r_{11}^2 + r_{12}^2 + r_{13}^2)^4 = \tfrac{N}{9}.
\end{aligned}
$$

In the derivations above, we substitute D-optimal values of the moments and use the properties of a rotation matrix. Using a similar approach, the proof for other moments can be obtained.

CHAPTER 4

Conclusion and Future Work

In this thesis, the problem of optimal GES design for second order DTI was reformulated as an experiment design problem (EDP). This EDP is a non-convex optimization problem. It is then converted into a convex SDP using convex relaxation. The proposed method guarantees a globally optimal solution and leads to several important theoretical results. Then, the proposed method is extended to optimal GES design for fourth order DTI and diffusion kurtosis imaging. It is also applied to ADC imaging. Several interesting findings, in addition to the new theoretical findings relating to optimal GES design, include: (i) among design approaches offered by experiment design theory, it is the D-optimal design that leads to rotation-invariant and UD GESs; (ii) the uniform distribution of gradient encoding directions is a necessity for D-optimal diffusion imaging when the number of measurements is nearly equal to the number of unknown model parameters; (iii) there exist UD designs that are simultaneously D-optimal for several models; and (iv) the proposed D-optimal design method improves the precision of estimated parameters compared to state-of-the-art methods;

The following points highlight the contributions and potential impact of this thesis: (i) an exact/analytical solution is of scientific interest even if approximate solutions are available. The difference between the proposed method and the existing UD solutions is more pronounced when using higher order models; (ii) a theoretically motivated method can be extended to similar problems; (iii) extension of the proposed method to high order models that require multi-shell acquisition adds further support to the utility of the proposed method; (iv) simultaneous optimality for several models means that several parties using different models can have the same optimal GES for data acquisition; (v) the proposed method

does not require any prior information (in contrast to some of the existing methods); and (vi) the proposed method can optimize both gradient encoding directions and *b*-values in multi-shell acquisitions.

Future Work

Further extension of the proposed work to higher order dMRI models provides scope for future work. Another possible avenue for future work is the extension of the proposed work to high order models (other than DKI) that require multi-shell acquisition. However, before proceeding with further theoretical developments, it is recommended that the existing theoretical results be validated using real data. Currently, the proposed method cannot be applied to non-linear model estimation. Extensions/modifications that allow experiment design for non-linear models can be an important topic for dMRI research.

Bibliography

[1] Klaus-Dietmar Merboldt, Wolfgang Hanicke, and Jens Frahm. Self-diffusion NMR imaging using stimulated echoes. *Journal of Magnetic Resonance (1969)*, 64(3):479 – 486, 1985.

[2] D. Lebihan and E. Breton. Imagerie de Diffusion In Vivo par Résonance Magnétique Nucléaire. *C R Académie des Sciences de Paris*, 301(15):1109–1112, 1985.

[3] Catherine Lebel, Thomas Benner, and Christian Beaulieu. Six is enough? comparison of diffusion parameters measured using six or more diffusion-encoding gradient directions with deterministic tractography. *Magnetic Resonance in Medicine*, 68(2):474–483, 2012.

[4] Wikimedia Commons. Philips MRI Scanner in Sahlgrenska Universitetsjukhuset, Gothenburg, Sweden, October 2015, available online at https://upload.wikimedia.org/wikipedia/commons/e/ee/MRI-Philips.JPG.

[5] Wikimedia Commons. Diffusion MRI Tractography in the Brain White Matter, October 2015, available online at https://commons.wikimedia.org/wiki/File:White_Matter_Connections_Obtained_with_MRI_Tractography.png.

[6] Wikimedia Commons. Superior Segment of the Bilateral Cingulum Bundles: Tractography Visualizations of Diffusion MRI Data, October 2015, available online at: https://commons.wikimedia.org/wiki/File:Superior_segment_of_the_bilateral_cingulum_bundles_(a).png.

[7] R. Woodhams, S. Ramadan, P. Stanwell, S. Sakamoto, H. Hata, M. Ozaki, S. Kan, and Y. Inoue. Diffusion-weighted Imaging of the Breast: Principles and Clinical Applications. *Radiographics*, 31:1059–1085, 2011.

[8] Dow-Mu Koh and David J. Collins. Diffusion-weighted MRI in the body: applications and challenges in oncology. *American Journal of Roentgenology*, 188(6):1622 – 1635, 2007.

[9] Yoshifumi Noda, Masayuki Kanematsu, Satoshi Goshima, Yukio Horikawa, Jun Takeda, Hiroshi Kondo, Haruo Watanabe, Hiroshi Kawada, Nobuyuki Kawai, Yukichi Tanahashi, and Kyongtae T Bae. Diffusion kurtosis imaging of the pancreas for the assessment of HbA1c levels. *Journal of Magnetic Resonance Imaging*, pages –, 2015.

[10] Carole Frindel, Marc Robini, Pierre Croisille, and Yue-Min Zhu. Comparison of regularization methods for human cardiac diffusion tensor MRI. *Medical Image Analysis*, 13(3):405 – 418, 2009.

[11] Benoit Scherrer and Simon K. Warfield. Parametric Representation of Multiple White Matter Fascicles from Cube and Sphere Diffusion MRI. *PLoS ONE*, 7(11), 2012.

[12] Daniel Alexander. An Introduction to Computational Diffusion MRI: the Diffusion Tensor and Beyond. *Visualization and Processing of Tensor Fields*, pages 83–106, 2007.

[13] Patric Hagmann, Lisa Jonasson, Philippe Maeder, Jean-Philippe Thiran, Van J. Wedeen, and Reto Meuli. Understanding diffusion mr imaging techniques: From scalar diffusion-weighted imaging to diffusion tensor imaging and beyond. *RadioGraphics*, 26(1):S205–S223, 2006.

[14] P. J. Basser, J. Mattiello, and D. LeBihan. MR diffusion tensor spectroscopy and imaging. *Biophysical journal*, 66(1):259–267, 1994.

[15] E. Özarslan and T. H. Mareci. Generalized diffusion tensor imaging and analytical relationships between diffusion tensor imaging and high angular resolution diffusion imaging. *Magn Reson Med*, 50(5):955–965, 2003.

[16] Jens H. Jensen, Joseph A. Helpern, Anita Ramani, Hanzhang Lu, and Kyle Kaczynski. Diffusional kurtosis imaging: The quantification of non-gaussian water diffusion by means of magnetic resonance imaging. *Magnetic Resonance in Medicine*, 53(6):1432–1440, 2005.

[17] Hanzhang Lu, Jens H. Jensen, Anita Ramani, and Joseph A. Helpern. Three-dimensional characterization of non-gaussian water diffusion in humans using diffusion kurtosis imaging. *NMR in Biomedicine*, 19(2):236–247, 2006.

[18] Stephen Boyd and Lieven Vandenberghe. *Convex Optimization*. Cambridge University Press, New York, NY, USA, 2004.

[19] Jane J. Ye and Julie Zhou. Minimizing the condition number to construct design points for polynomial regression models. *SIAM J. Optim.*, 23(1):666–686, 2013.

[20] Nikolaos G. Papadakis, Da Xing, Christopher L. H. Huang, Laurance D. Hall, and Adrian T. Carpenter. A comparative study of acquisition schemes for diffusion tensor imaging using MRI. *Journal of Magnetic Resonance*, 137(1):67–82, 1999.

[21] Nikolaos G Papadakis, Chris D Murrills, Laurance D Hall, Christopher L. Huang, and T Adrian Carpenter. Minimal gradient encoding for robust estimation of diffusion anisotropy. *Magnetic Resonance Imaging*, 18(6):671 – 679, 2000.

[22] Stefan Skare, Tie-Qiang Li, Bo Nordell, and Martin Ingvar. Noise considerations in the determination of diffusion tensor anisotropy. *Magnetic Resonance Imaging*, 18(6):659 – 669, 2000.

[23] Khader M. Hasan, Peter J. Basser, Dennis L. Parker, and Andrew L. Alex. Analytical computation of the eigenvalues and eigenvectors in DT-MRI. *J. Magn. Reson*, pages 41–47, 2001.

[24] Khader M Hasan, Dennis L Parker, and Andrew L Alexander. Magnetic resonance water self-diffusion tensor encoding optimization methods for full brain acquisition. *Image Analysis and Stereology*, 21(2):87–96, 2002.

[25] Dubois, J., Poupon, C., Lethimonnier, F., Le Bihan, and D. Optimized diffusion gradient orientation schemes for corrupted clinical DTI data sets. *MAGMA Magnetic Resonance Materials in Physics, Biology and Medicine*, 19(3):134–143, 2006.

[26] Khader M. Hasan. A framework for quality control and parameter optimization in diffusion tensor imaging: theoretical analysis and validation. *Magnetic Resonance Imaging*, 25(8):1196 – 1202, 2007.

[27] Sarah C. Mang, Daniel Gembris, Wolfgang Grodd, and Uwe Klose. Comparison of gradient encoding directions for higher order tensor diffusion data. *Magnetic Resonance in Medicine*, 61(2):335–343, 2009.

[28] D. K. Jones, M. A. Horsfield, and A. Simmons. Optimal strategies for measuring diffusion in anisotropic systems by magnetic resonance imaging. *Magnetic Resonance in Medicine*, 42:515–525, 1999.

[29] Derek K. Jones. *Diffusion MRI theory, methods, and applications*. Oxford University Press, 2011.

[30] Emmanuel Caruyer and Rachid Deriche. A Computational Framework for Experimental Design in Diffusion MRI. In *CDMRI - MICCAI Workshop on Computational Diffusion MRI*, Nice, France, 2012.

[31] D. K. Jones. The effect of gradient sampling schemes on measures derived from diffusion tensor MRI: A Monte Carlo study. *Magnetic Resonance in Medicine*, 51:807–815, 2004.

[32] P.G. Batchelor, D. Atkinson, D.L.G. Hill, F. Calamante, and A. Connelly. Anisotropic noise propagation in diffusion tensor MRI sampling schemes. *Magn Reson Med*, 49(6):1143–51, 2003.

[33] P. A. Narayana K. M. Hasan. DTI parameter optimization at 3.0 T: potential application in entire normal human brain mapping and multiple sclerosis research. *MEDICAMUNDI*, 49(1):30–45, 2005.

[34] Shantanu Majumdar, David C. Zhu, Satish S. Udpa, and L. Guy Raguin. A diffusion gradient optimization framework for spinal cord diffusion tensor imaging. *Magnetic Resonance Imaging*, 29(6):789 – 804, 2011.

[35] Wei Gao, Hongtu Zhu, and Weili Lin. A unified optimization approach for diffusion tensor imaging technique. *NeuroImage*, 44(3):729 – 741, 2009.

[36] David S. Tuch. Q-ball imaging. *Magn. Reson. Med.*, 52(6):1358–1372, 2004.

[37] KM Jansons and DC Alexander. Persistent angular structure: new insights from diffusion magnetic resonance imaging data. *Inverse Problems*, 19:1031–1046, 2003.

[38] Tim B. Dyrby, Lise V. Sogaard, Matt G. Hall, Maurice Ptito, and Daniel. C. Alexander. Contrast and stability of the axon diameter index from microstructure imaging with diffusion MRI. *Magnetic Resonance in Medicine*, 70(3):711–721, 2013.

[39] Yaniv Assaf, Raisa Z. Freidlin, Gustavo K. Rohde, and Peter J. Basser. New modeling and experimental framework to characterize hindered and restricted water diffusion in brain white matter. *Magnetic Resonance in Medicine*, 52(5):965–978, 2004.

[40] Yaniv Assaf, Tamar Blumenfeld-Katzir, Yossi Yovel, and Peter J. Basser. Axcaliber: A method for measuring axon diameter distribution from diffusion MRI. *Magnetic Resonance in Medicine*, 59(6):1347–1354, 2008.

[41] S. De Santis, Y. Assaf, C. J. Evans, and D. K. Jones. Improved precision in CHARMED assessment of white matter through sampling scheme optimization and model parsimony testing. *Magnetic Resonance in Medicine*, 71(2):661–671, 2014.

[42] Daniel C. Alexander. A general framework for experiment design in diffusion MRI and its application in measuring direct tissue-microstructure features. *Magnetic Resonance in Medicine*, 60(2):439–448, 2008.

[43] Dirk H. J. Poot, Arnold Jan den Dekker, Eric Achten, Marleen Verhoye, and Jan Sijbers. Optimal experimental design for diffusion kurtosis imaging. *IEEE Transactions on Medical Imaging*, 29(3):819–829, 2010.

[44] Emmanuel Caruyer, Christophe Lenglet, Guillermo Sapiro, and Rachid Deriche. Design of multishell sampling schemes with uniform coverage in diffusion MRI. *Magnetic Resonance in Medicine*, 69(6):1534–1540, April 2013.

[45] Cheng Guan Koay, Evren Özarslan, Kevin M. Johnson, and Mary Elizabeth Meyerand. Sparse and optimal acquisition design for diffusion MRI and beyond. *Medical Physics*, 39(5):2499–2511, 2012.

[46] Liang Zhan, Alex D. Leow, Iman Aganj, Christophe Lenglet, Guillermo Sapiro, Essa Yacoub, Noam Harel, Arthur W. Toga, and Paul M. Thompson. Differential information content in staggered multiple shell HARDI measured by the tensor distribution function. In *IEEE International Symposium on Biomedical Imaging ISBI*, pages 305–309, 2011.

[47] S. Skare, M. Hedehus, M.E. Moseley, and T.Q. Li. Condition number as a measure of noise performance of diffusion tensor data acquisition schemes with MRI. *J Magn Reson*, 147(2):340–52, 2000.

[48] Peter Savadjiev. *Perceptual organisation in diffusion MRI: curves and streamline flows*. PhD Thesis, McGill University, Montreal, Canada, 2008.

[49] David Raffelt. *Group Wise Analysis of High Angular Resolution Diffusion-Weighted Magnetic Resonance Images*. Confirmation Report, The University of Queensland, 2009.

[50] Wikimedia Commons. Neuron, November 2013, available online at: http://commons.wikimedia.org/wiki/File:Neuron.svg.

[51] Callaghan T. Paul. *Principles of Nuclear Magnetic Resonance Microscopy*. Oxford University Press, 1991.

[52] Maxime Descoteaux. *High Angular Resolution Diffusion MRI: from Local Estimation to Segmentation and Tractography*. PhD Thesis, University of Nice-Sophia Antipolis, 2008.

[53] Santiago Aja-Fernandez, Carlos Alberola-Lopez, and Carl-Fredrik Westin. Noise and signal estimation in magnitude MRI and rician distributed images: A LMMSE approach. *IEEE Transactions on Image Processing*, 17(8):1383–1398, 2008.

[54] Haz-Edine Assemlal, David Tschumperle, Luc Brun, and Kaleem Siddiqi. Recent advances in diffusion MRI modeling: Angular and radial reconstruction. *Medical Image Analysis*, 15(4):369–396, 2011.

[55] Van J. Wedeen, Patric Hagmann, Wen-Yih I. Tseng, Timothy G. Reese, and Robert M. Weisskoff. Mapping complex tissue architecture with diffusion spectrum magnetic resonance imaging. *Magn. Reson. Med.*, 54(6):1377–1386, 2005.

[56] Peter B. Kingsley. Introduction to diffusion tensor imaging mathematics: Part II. anisotropy, diffusion-weighting factors, and gradient encoding schemes. *Concepts in Magnetic Resonance Part A*, 28A(2):123–154, 2006.

[57] Divya Varadarajan and Justin P. Haldar. MS-FRACT: Optimized linear transform methods for ODF estimation in multi-shell diffusion MRI. *In Proceedings of ISBI15: IEEE International Symposium on Biomedical Imaging*, pages 1172–1175, 2015.

[58] F.J. Chen. *Progress in Brain Mapping Research*. Nova Science Publishers, Hauppauge NY, USA, 2006.

[59] Khader M. Hasan, Dennis L. Parker, and Andrew L. Alexander. Comparison of gradient encoding schemes for diffusion-tensor MRI. *Journal of Magnetic Resonance Imaging*, 13(5):769–780, 2001.

[60] L. Zhan et. al. How does angular resolution affect diffusion imaging measures? *NeuroImage*, 49(2):1357 – 1371, 2010.

[61] Derek K. Jones. Determining and visualizing uncertainty in estimates of fiber orientation from diffusion tensor MRI. *Magnetic Resonance in Medicine*, 49:7–12, 2003.

[62] E.O. Stejskal and J.E. Tanner. Spin diffusion measurements: Spin echoes in the presence of a time-dependent field gradient. *Journal of Chemical Physics*, 42(1):288–292, 1965.

[63] Emmanuel Caruyer, Jian Cheng, Christophe Lenglet, Guillermo Sapiro, Tianzi Jiang, and Rachid Deriche. Optimal Design of Multiple Q-shells experiments for Diffusion MRI. In *MICCAI Workshop on Computational Diffusion MRI - CDMRI'11*, Toronto, Canada, September 2011.

[64] Emmanuel Caruyer, Christophe Lenglet, Guillermo Sapiro, and Dr. Deriche, Rachid. Incremental gradient table for multiple Q-shells diffusion MRI. In *HBM 17th Annual Meeting*, Québec, Canada, June 2011.

[65] Hans Knutsson and Carl-Fredrik Westin. Tensor metrics and charged containers for 3D Q-space sample distribution. In *Medical Image Computing and Computer-Assisted Intervention - MICCAI*, Lecture Notes in Computer Science, 2013.

[66] A. Leemans, B. Jeurissen, J. Sijbers, and DK Jones. ExploreDTI: a graphical toolbox for processing, analyzing, and visualizing diffusion MR data. In *17th Annual Meeting of Intl Soc Mag Reson Med*, page 3537, 2009.

[67] Alexander Leemans. ExploreDTI image gallery, October 2015, available online at: http://www.exploredti.com/gallery/.

[68] David Raffelt. *Voxel-Based Analysis of High Angular Resolution Diffusion-Weighted Magnetic Resonance Images*. PhD Thesis, The University of Queensland, 2011.

[69] James G. Malcolm, Yogesh Rathi, and Carl-Fredrik Westin. Processing and visualization of diffusion MRI. In Thomas Martin Deserno, editor, *Biomedical Image Processing*, Biological and Medical Physics, Biomedical Engineering, pages 403–424. Springer Berlin Heidelberg, 2011.

[70] Min Jing, T. Martin McGinnity, Sonya A. Coleman, Huaizhong Zhang, Armin Fuchs, and J. A. Scott Kelso. Enhancement of fiber orientation distribution reconstruction in diffusion-weighted imaging by single channel blind source separation. *IEEE Trans. Biomed. Engineering*, 59(2):363–373, 2012.

[71] Eleftheria Panagiotaki, Torben Schneider, Bernard Siow, Matt G. Hall, Mark F. Lythgoe, and Daniel C. Alexander. Compartment models of the diffusion MR signal in brain white matter: A taxonomy and comparison. *NeuroImage*, 59(3):2241–2254, 2012.

[72] Evren Ozarslan, Timothy M. Shepherd, Baba C. Vemuri, Stephen J. Blackband, and Thomas H. Mareci. Resolution of complex tissue microarchitecture using the diffusion orientation transform (DOT). *NeuroImage*, 31(3):1086 – 1103, 2006.

[73] Baba C. Vemuri Bing Jian. A unified computational framework for deconvolution to reconstruct multiple fibers from diffusion weighted MRI. *IEEE Trans. Med. Imaging*, 26(11):1464–1471, 2007.

[74] A. Barmpoutis et. al. Regularized positive-definite fourth-order tensor field estimation from DW-MRI. *NeuroImage*, 45(1 sup.1):153–162, 2009.

[75] Iman Aganj, Christophe Lenglet, and Guillermo Sapiro. ODF maxima extraction in spherical harmonic representation via analytical search space reduction. In *MICCAI (2)*, volume 6362 of *Lecture Notes in Computer Science*, pages 84–91. Springer, 2010.

[76] Aurobrata Ghosh, Elias Tsigaridas, Bernard Mourrain, and Rachid Deriche. A polynomial approach for extracting the extrema of a spherical function and its application in diffusion MRI. *Medical Image Analysis*, 17(5):503–514, 2013.

[77] Aurobrata Ghosh, P. Tsigaridas, Elias P., Maxime Descoteaux, Pierre Comon, Bernard Mourrain, and Rachid Deriche. A Polynomial based approach to extract the maxima of an antipodally symmetric spherical function and its application to extract fiber directions from the Orientation Distribution Function in Diffusion MRI. In *11th International Conference on Medical Image Computing and Computer Assisted Intervention (MICCAI)*, pages 237–248, 2008.

[78] F. Jiao et. al. Detection of crossing white matter fibers with high-order tensors and rank-k decompositions. In *Proc 22nd Int Conf Information processing in medical imaging*, IPMI'11, pages 538–549, Berlin, Heidelberg, 2011. Springer-Verlag.

[79] L. Qi, G. Yu, and E. Wu. Higher order positive semidefinite diffusion tensor imaging. *SIAM Journal on Imaging Sciences*, 3(3):416–433, 2010.

[80] Liqun Qi, Gaohang Yu, and Yi Xu. Nonnegative diffusion orientation distribution function. *Journal of Mathematical Imaging and Vision*, 45(2):103–113, 2013.

[81] Yonas T. Weldeselassie, Angelos Barmpoutis, and M. Stella Atkins. Symmetric positive-definite cartesian tensor orientation distribution functions (CT-ODF). In *Proceedings of the 13th International Conference on Medical Image Computing and Computer-assisted Intervention: Part I*, MICCAI'10, pages 582–589, 2010.

[82] ISBI2012. HARDI reconstruction contest, October 2013, available online at: http://hardi.epfl.ch/static/events/2012_ISBI/.

[83] MICCAI2013. Computational diffusion MRI challenge, October 2013, http://cmic.cs.ucl.ac.uk/miccai13wmm/.

[84] Aurobrata Ghosh and Rachid Deriche. 4th order symmetric tensors and positive ADC modelling. In Anna Vilanova, Carl-Fredrik Westin, and Bernhard Burgeth, editors, *Visualization and Processing of Tensors and Higher Order Descriptors for Multi-Valued Data (Dagstuhl Seminar 11501)*. Springer, 2013.

[85] M. Alipoor, I. Y.H. Gu, A. J.H. Mehnert, Y. Lilja, and D. Nilsson. On high order tensor-based diffusivity profile estimation. In *Engineering in Medicine and Biology Society (EMBC), 2013 35th Annual International Conference of the IEEE*, pages 93–96, 2013.

[86] A. Barmpoutis and B. C. Vemuri. A unified framework for estimating diffusion tensors of any order with symmetric positive-definite constraints. *Proc IEEE Int Symp Biomed Imaging*, pages 1385–1388, 2010.

[87] L. Qi. The spectral theory of tensors (rough version). *arXiv preprint arXiv:1201.3424*, 2012.

[88] Ed X. Wua and Matthew M. Cheung. MR diffusion kurtosis imaging for neural tissue characterization. *NMR Biomed*, 23(7):836–848, 2009.

[89] Jiachen Zhuo, Su Xu, Julie L. Proctor, Roger J. Mullins, Jonathan Z. Simon, Gary Fiskum, and Rao P. Gullapalli. Diffusion kurtosis as an in vivo imaging marker for reactive astrogliosis in traumatic brain injury. *NeuroImage*, 59(1):467 – 477, 2012.

[90] Matthew M. Cheung, Edward S. Hui, Kevin C. Chan, Joseph A. Helpern, Liqun Qi, and Ed X. Wu. Does diffusion kurtosis imaging lead to better

neural tissue characterization? A rodent brain maturation study. *NeuroImage*, 45(2):386 – 392, 2009.

[91] Jiajia Zhu, Chuanjun Zhuo, Wen Qin, Di Wang, Xiaomei Ma, Yujing Zhou, and Chunshui Yu. Performances of diffusion kurtosis imaging and diffusion tensor imaging in detecting white matter abnormality in schizophrenia. *NeuroImage: Clinical*, 7(0):170 – 176, 2015.

[92] Ali Tabesh, Jens H. Jensen, Babak A. Ardekani, and Joseph A. Helpern. Estimation of tensors and tensor-derived measures in diffusional kurtosis imaging. *Magnetic Resonance in Medicine*, 65(3):823–836, 2011.

[93] R.N. Sener. Diffusion MRI: apparent diffusion coefficient (ADC) values in the normal brain and a classification of brain disorders based on ADC values. *Computerized Medical Imaging and Graphics*, 25(4):299 – 326, 2001.

[94] Wael Abdulghaffar and Magdy M. Tag-Aldeen. Role of diffusion-weighted imaging (DWI) and apparent diffusion coefficient (ADC) in differentiating between benign and malignant breast lesions. *The Egyptian Journal of Radiology and Nuclear Medicine*, 44(4):945 – 951, 2013.

[95] Jian-Min Shen, Xian-Wu Xia, Wu-Gen Kang, Jian-Jun Yuan, and Liang Sheng. The use of MRI apparent diffusion coefficient (ADC) in monitoring the development of brain infarction. *BMC Medical Imaging*, 11:2+, January 2011.

[96] Jeff L. Zhang, Eric E. Sigmund, Hersh Chandarana, Henry Rusinek, Qun Chen, Pierre-Hugues Vivier, Bachir Taouli, and Vivian S. Lee. Variability of renal apparent diffusion coeffi cients: Limitations of the monoexponential model for diffusion quantification. *Radiology*, 254(3):783 – 792, 2010.

[97] Bozkurt Y et al. Göya C, Hamidi C. The role of apparent diffusion coefficient quantification in differentiating benign and malignant renal masses by 3 Tesla magnetic resonance imaging. *Balkan Medical Journal*, 32(3):273–278, 2006.

[98] Sally Emad-Eldin, Manal Halim, Lamiaa I.A. Metwally, and Rania Mahmoud Abdel-Aziz. Diffusion-weighted MR imaging and ADC measurement in normal prostate, benign prostatic hyperplasia and prostate carcinoma. *The Egyptian Journal of Radiology and Nuclear Medicine*, 45(2):535 – 542, 2014.

[99] Michael A. Jacobs, Ronald Ouwerkerk, Kyle Petrowski, and Katarzyna J. Macura. Diffusion-weighted imaging with apparent diffusion coefficient mapping and spectroscopy in prostate cancer. *Top Magn Reson Imaging*, 19(6):261 – 272, 2008.

[100] Naoko Mukuda, Shinya Fujii, Chie Inoue, Takeru Fukunaga, Yoshio Tanabe, Hiroaki Itamochi, and Toshihide Ogawa. Apparent diffusion coefficient (ADC) measurement in ovarian tumor: Effect of region-of-interest methods on ADC values and diagnostic ability. *Journal of Magnetic Resonance Imaging*, pages n/a–n/a, 2015.

[101] Khaled A. Ahmad and Ahmed Abdrabou. The significance of added ADC value to conventional MR imaging in differentiation between benign and malignant ovarian neoplasms. *The Egyptian Journal of Radiology and Nuclear Medicine*, 45(3):997 – 1002, 2014.

[102] Kazumichi Tsukamoto, Eiji Matsusue, Yoshiko Kanasaki, Suguru Kakite, Shinya Fujii, Toshio Kaminou, and Toshihide Ogawa. Significance of apparent diffusion coefficient measurement for the differential diagnosis of multiple system atrophy, progressive supranuclear palsy, and parkinson's disease: evaluation by 3.0-T MR imaging. *Neuroradiology*, 54(9):947–955, 2012.

[103] Hai-Feng Li et al. Yu Lei, Hong Wang. Diagnostic significance of diffusion-weighted MRI in renal cancer. *BioMed Research International*, 2015(ID 172165):12, 2006.

[104] Akio Ogura, Katsumi Hayakawa, Tosiaki Miyati, and Fumie Maeda. Imaging parameter effects in apparent diffusion coefficient determination of magnetic resonance imaging. *European Journal of Radiology*, 77(1):185 – 188, 2011.

[105] Takeshi Yoshikawa, Hideaki Kawamitsu, Donald G. Mitchell, Yoshiharu Ohno, Yonson Ku, Yasushi Seo, Masahiko Fujii, and Kazuro Sugimura. ADC measurement of abdominal organs and lesions using parallel imaging technique. *American Journal of Roentgenology*, 187(6):1521–1530, 2006.

[106] Thoeny Harriet C. Koh, Dow-Mu. *Diffusion-Weighted MR Imaging: Applications in the Body*. Springer-Verlag Berlin Heidelberg, 2010.

[107] Erik Sjögren, Joakim Nyberg, Mats O. Magnusson, Hans Lennernäs, Andrew Hooker, and Ulf Bredberg. Optimal experimental design for assessment of enzyme kinetics in a drug discovery screening environment. *Drug Metabolism and Disposition*, 39(5):858–863, 2011.

[108] Anders Kristoffersen. Diffusion measurements and diffusion tensor imaging with noisy magnitude data. *Journal of Magnetic Resonance Imaging*, 29(1):237–241, 2009.

[109] Jing Yuan, David Ka Wai Yeung, Greta S. P. Mok, Kunwar S. Bhatia, Yi-Xiang J. Wang, Anil T. Ahuja, and Ann D. King. Non-gaussian analysis of diffusion weighted imaging in head and neck at 3T: A pilot study in patients with nasopharyngeal carcinoma. *PLoS ONE*, 9(1):e87024, 01 2014.

[110] J.F.A. Jansen, H.E. Stambuk, J.A. Koutcher, and A. Shukla-Dave. Non-gaussian analysis of diffusion-weighted MR imaging in head and neck squamous cell carcinoma: A feasibility study. *American Journal of Neuroradiology*, 31(4):741–748, 2010.

[111] Bito Y, Hirata S, and Yamamoto E. Optimum gradient factors for apparent diffusion coefficient measurements. *Proc SMR/ESMRMB Joint Meeting, Nice*, page 913, 1995.

[112] Da Xing, Nikolaos G. Papadakis, Christopher L.-H. Huang, Vee Meng Lee, T. Adrian Carpenter, and Laurance D. Hall. Optimised diffusion-weighting for measurement of apparent diffusion coefficient (ADC) in human brain. *Magnetic Resonance Imaging*, 15(7):771 – 784, 1997.

[113] Oscar Brihuega-Moreno, Frank P. Heese, and Laurance D. Hall. Optimization of diffusion measurements using Cramer-Rao lower bound theory and its application to articular cartilage. *Magnetic Resonance in Medicine*, 50(5):1069–1076, 2003.

[114] Steve Smith. Introduction to the neuroimage special issue "Mapping the Connectome". *NeuroImage*, 80(0):1–1, 2013.

[115] Marco Reisert, Irina Mader, Constantin Anastasopoulos, Matthias Weigel, Susanne Schnell, and Valerij Kiselev. Global fiber reconstruction becomes practical. *NeuroImage*, 54(2):955 – 962, 2011.

[116] Longchuan Li, James K. Rilling, Todd M. Preuss, Matthew F. Glasser, Frederick W. Damen, and Xiaoping Hu. Quantitative assessment of a framework for creating anatomical brain networks via global tractography. *NeuroImage*, 61(4):1017 – 1030, 2012.

[117] J.-F. Mangin, P. Fillard, Y. Cointepas, D. Le Bihan, V. Frouin, and C. Poupon. Toward global tractography. *NeuroImage, Mapping the Connectome*, 80(0):290 – 296, 2013.

[118] Marco Reisert, Irina Mader, Roza Umarova, Simon Maier, Ludger Tebartz van Elst, and Valerij G. Kiselev. Fiber density estimation from single q-shell diffusion imaging by tensor divergence. *NeuroImage*, 77(0):166 – 176, 2013.

[119] Marco Reisert and Valerij G. Kiselev. Fiber continuity: An anisotropic prior for odf estimation. *IEEE Trans. Med. Imaging*, 30(6):1274–1283, 2011.

[120] Luke Bloy and Ragini Verma. On computing the underlying fiber directions from the diffusion orientation distribution function. *Med Image Comput Comput Assist Interv*, 11(Pt 1):1–8, 2008.

[121] Maxime Descoteaux, Rachid Deriche, Thomas R. KnÃűsche, and Alfred Anwander. Deterministic and probabilistic tractography based on complex fibre orientation distributions. *IEEE Trans. Med. Imaging*, 28(2):269–286, 2009.

[122] Marco Reisert, Elias Kellner, and Valerij G. Kiselev. About the geometry of asymmetric fiber orientation distributions. *IEEE Trans. Med. Imaging*, 31(6):1240–1249, 2012.

[123] Nathan S. Hageman, Arthur W. Toga, Katherine Narr, and David W. Shattuck. A diffusion tensor imaging tractography algorithm based on navier-stokes fluid mechanics. *IEEE Trans. Med. Imaging*, 28(3):348–360, 2009.

[124] Andrew Zalesky. DT-MRI fiber tracking: A shortest paths approach. *IEEE Trans. Med. Imaging*, 27(10):1458–1471, 2008.

[125] Robert E. Smith, Jacques-Donald Tournier, Fernando Calamante, and Alan Connelly. SIFT: Spherical-deconvolution informed filtering of tractograms. *NeuroImage*, 67:298–312, 2013.

[126] Burak Yoldemir, Burak Acar, Zeynep Firat, and Ozgur Kilickesmez. SMT: A reliability based interactive DTI tractography algorithm. *IEEE Trans. Med. Imaging*, 31(10):1929–1940, 2012.

[127] Pew-Thian Yap, John H. Gilmore, Weili Lin, and Dinggang Shen. PopTract: Population-based tractography. *IEEE Trans. Med. Imaging*, 30(10):1829–1840, 2011.

[128] Marco Reisert, Irina Mader, and Valerij Kiselev. Global reconstruction of neuronal fibres. In *In Proceedings of MICCAI, Diffusion Modelling Workshop. 2009*.

[129] Kei Yamada, Koji Sakai, Kentaro Akazawa, Sachiko Yuen, and Tsunehiko Nishimura. MR tractography: A review of its clinical applications. *Magnetic Resonance in Medical Sciences*, 8(4):165–174, 2009.

[130] Saad Jbabdi and Heidi Johansen-Berg. Tractography: where do we go from here? *Brain connectivity*, 1(3):169–183, 2011.

[131] P. Fillard et. al. Quantitative evaluation of 10 tractography algorithms on a realistic diffusion MR phantom. *NeuroImage*, 56(1):220–34, 2011.

[132] Ting-Shuo Yo, Alfred Anwander, Maxime Descoteaux, Pierre Fillard, Cyril Poupon, and Thomas R. KnÃűsche. Quantifying brain connectivity: A comparative tractography study. In Guang-Zhong Yang, David J. Hawkes, Daniel Rueckert, J. Alison Noble, and Chris J. Taylor, editors, *MICCAI (1)*, volume 5761 of *Lecture Notes in Computer Science*, pages 886–893. Springer, 2009.

[133] Zhaosong Lu and Ting Kei Pong. Minimizing condition number via convex programming. *SIAM J. Matrix Analysis Applications*, 32(4):1193–1211, 2011.

[134] Mohammad Alipoor, Irene Yu-Hua Gu, Andrew J. H. Mehnert, Ylva Lilja, and Daniel Nilsson. Optimal diffusion tensor imaging with repeated measurements. In *MICCAI (1)*, volume 8149 of *Lecture Notes in Computer Science*, pages 687–694. Springer, 2013.

[135] D. Rea R. Moineddin L. Vidarsson E. Widjaja, S. Z. Mahmoodabadi and D. Nilsson. Effects of Gradient Encoding and Number of Signal Averages on Fractional Anisotropy and Fiber Density Index In Vivo at 1.5 Tesla. *Acta Radiologica*, 50(1):106–113, 2009.

[136] A. Yamamoto, Y. Miki, S. Urayama, Y. Fushimi, T. Okada, T. Hanakawa, H. Fukuyama, and K. Togashi. Diffusion Tensor Fiber Tractography of the Optic Radiation: Analysis with 6-, 12-, 40-, and 81-Directional Motion-Probing Gradients, a Preliminary Study. *AJNR Am J Neuroradiol*, 28(1):92–96, 2007.

[137] H. Ni, V. Kavcic, T. Zhu, S. Ekholm, and J. Zhong. Effects of number of diffusion gradient directions on derived diffusion tensor imaging indices in human brain. *AJNR. American journal of neuroradiology*, 27(8):1776–1781, 2006.

[138] Jun Yi Wang, Hervé Abdi, Khamid Bakhadirov, Ramon Diaz-Arrastia, and Michael D. Devous Sr. A comprehensive reliability assessment of quantitative diffusion tensor tractography. *NeuroImage*, 60(2):1127–1138, 2012.

[139] Bennett A. Landman, Jonathan A. D. Farrell, Craig K. Jones, Seth A. Smith, Jerry L. Prince, and Susumu Mori. Effects of diffusion weighting schemes on the reproducibility of DTI-derived fractional anisotropy, mean diffusivity, and principal eigenvector measurements at 1.5T. *Neuroimage*, 36(4):1123–1138, 2007.

[140] Jan Sijbers and Arjan den Dekker. Maximum likelihood estimation of signal amplitude and noise variance from MR data. *Magnetic Resonance in Medicine*, 51(3):586–594, 2004.